J. Fluid Mech. (1982), *vol.* 124, *pp.* 173–207
Printed in Great Britain

Mechanisms of inlet-vortex formation

By F. DE SIERVI, H. C. VIGUIER, E. M. GREITZER AND C. S. TAN
Massachusetts Institute of Technology, Cambridge, Massachusetts 02139

(Received 2 October 1981 and in revised form 14 May 1982)

An experimental and theoretical study is presented of the inlet-vortex (or ground-vortex) phenomenon. The experiments were carried out in a water tunnel using hydrogen-bubble flow visualization. The theoretical study is based on a secondary-flow approach in which vortex filaments in a (weak) shear flow are viewed as convected (and deformed) by a three-dimensional irrotational primary flow; the latter being calculated numerically using a three-dimensional panel method. Two basic mechanisms of inlet-vortex generation are identified. The first of these, which has been alluded to qualitatively by other investigators, is the amplification of ambient (i.e. far-upstream) vorticity as the vortex lines are stretched and drawn into the inlet. Quantitative calculations have been carried out to illustrate the central features connected with this amplification. In contrast with what has been supposed, however, there is another mechanism of inlet-vortex formation, which does not appear to have been recognized previously and which does not require the presence of ambient vorticity. It is thus shown that an inlet vortex can arise in an (upstream) irrotational flow, for an inlet in cross wind. In this situation, the vortex is accompanied by a variation in circulation along the length of the inlet. The ratio of inlet velocity to upstream velocity is an important parameter for both mechanisms.

1. Introduction

1.1. *Background*

When a gas-turbine engine is operated near a ground plane at static or near-static conditions, a strong vortex is often observed to form between the ground and the inlet. This so called inlet vortex (or ground vortex) can cause severe operational difficulties. It can cause loose debris to be picked up from the ground and drawn into the engine, and can also create flow distortions at the engine face that adversely affect the aerodynamic stability of the engine compression system. The potential for vortex-induced compressor surge has risen with the use of wide-body aircraft powered by high-bypass-ratio turbofans, since in these configurations the distortion occupies more of the core compressor flow area and the engines are closer to the ground than in the past.

An inlet vortex produces a flow that has a large-amplitude flow angle and velocity distortion over a considerable extent of the engine face. There is, however, a significant total pressure defect only over a small fraction of the inlet flow-through area; i.e. only in the vortex core. Thus the decrease in engine stall margin due to this type of distortion cannot be predicted by present analyses of compressor response to non-uniform inlet flow, since these are all aimed at roughly unidirectional motions with large extent total pressure distortions (Greitzer 1980).

Initially because of the ingestion problem, and more recently because of the effect

on engine stability, the inlet-vortex phenomenon has been examined by many investigators. These have included small-scale experiments (e.g. Klein 1957; Glenny 1970; Motycka, Walter & Muller 1973; Motycka & Walter 1975; Bissinger & Braun 1974), full-scale tests with engines (Rodert & Garrett 1955; Motycka 1976), panel-method calculations of the velocity field associated with a potential vortex and inlet combination (Colehour & Farquhar 1971), and two-dimensional free-streamline potential-flow models of an inlet near a ground plane (Newman & Atassi 1980).

A discussion of these various studies is given by Viguier (1980), but we can summarize the main conclusions presented in the existing literature as follows. First, it is assumed that an inlet vortex can form only if ambient vorticity exists in the fluid drawn into the inlet. By the term 'ambient vorticity' we mean vorticity created at a *far-upstream location*, where the existence of the vorticity is essentially *independent of the presence of the inlet*. One obvious example of this type of ambient vorticity is the shear flow that occurs when a wind blows across and airfield. Another results from the use of a fan or propeller to provide a non-uniform, rotational, flow into an inlet, as was done in several of the experiments described in the references.

The second conclusion is that the existence of a stagnation point on the ground near the front of the inlet is believed to be required for the phenomenon to appear. Also, the inlet vortex, which can be part of a system of vortices, may be unsteady. Further, the thin boundary layer due to the inlet (sink flow) alone is not essential in the vortex formation. The following parameters have been used to characterize this phenomenon: ratio V_i/V_∞ of inlet throat velocity to ambient wind velocity, ratio H/D of inlet centreline height to inlet diameter, wind direction, and the ratio of the inlet velocity to the product of centreline far-upstream wind velocity gradient and inlet diameter (this is a rough measure of the magnitude of the ambient vorticity). In particular, increasing the first ratio or decreasing the second and fourth has been found to result in either an increased tendency for a vortex to form, or the strengthening of an existing vortex.

In spite of the work that has been done on this topic, the fundamental fluid-mechanical processes responsible for the generation of the inlet vortex are still not well understood. For example, if we accept the hypothesis that the formation of the inlet vortex is due to the intensification (amplification) of ambient vorticity as it is drawn into the inlet, a basic question arises. If we consider the fluid to be inviscid and of constant density, and examine the ingestion into the inlet of vortex lines that have originated far upstream, the process might appear somewhat as sketched in figure 1, which shows a vortex line at three instants of time. Since vortex lines cannot end in the fluid, the two 'legs' that are ingested must possess an equal and opposite *circulation* (although the vorticity may be different owing to the different amounts of stretching undergone by the two legs). In practice, however, only one vortex is observed. It is possible that the other leg could appear as a thin layer of streamwise vorticity, 'smeared' on the inner wall of the inlet. However, it is not certain that this actually does occur (and in fact we will see below that this is not the case). In addition to this basic question, quantitative relationships between the overall flow parameters presented above and the engine face velocity distribution, which is the information necessary to assess compressor stall margin decrease, do not exist. The desire to examine these topics prompted this study.

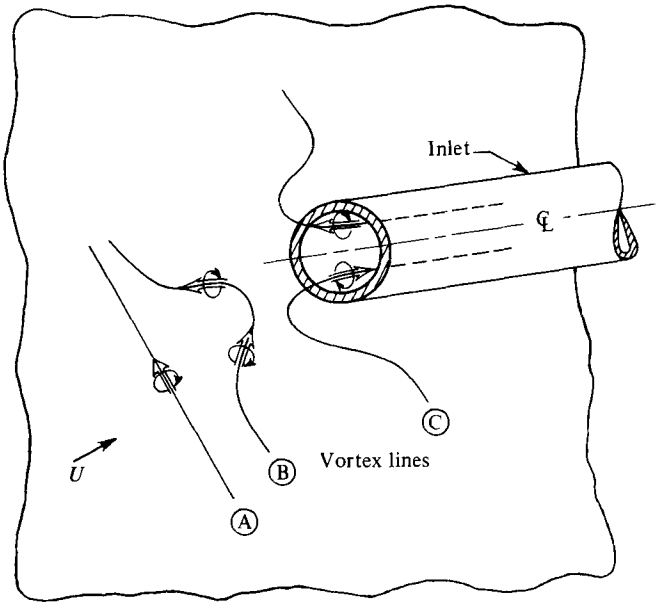

FIGURE 1. Ingestion of a vortex line into an inlet: sketch of the vortex line at three successive times $t_A < t_B < t_C$.

1.2. *Scope and organization of the paper*

The organization of the paper is somewhat different from usual for the following reasons. When we embarked on this project, the view of the problem was that intensification of ambient vorticity was responsible for vortex formation. Secondary-flow calculations (described below) confirmed this idea.

When we carried out the experiments, it became clear that this view of the phenomenon was not complete. The experiments did show that one cause, or mechanism, for the formation of inlet vortices was indeed this intensification of the ambient vorticity. However, they also showed, contrary to what had been previously supposed, that an inlet vortex can form in a flow that is *irrotational* (uniform) far upstream of the inlet. Anticipating the overall conclusions of the paper, therefore, we state that there are two basically different causes (or mechanisms) of inlet-vortex formation, and we have organized the paper around the two different physical processes.

In the paper the conceptual design of the experiments and the experimental facility are first described. The specific experiments to illustrate the first mechanism (the amplification of ambient vorticity) are then presented, followed by a secondary-flow analysis of the three-dimensional vorticity field around the inlet. This set of experiments and the accompanying analysis is focused on the situation in which the inlet faces directly into the upstream flow, because with this configuration the mechanism under discussion is most clearly shown.

Following this, the results of the experiments relating to the second mechanism, which is responsible for inlet-vortex formation in an upstream irrotational flow, are presented. This set of experiments involves an inlet in operation with its axis perpendicular to the mean flow, so that the inlet is in 'cross wind'. The experiments include tests carried out with an inlet near a ground plane, as well as tests with a twin-inlet configuration, so that no 'ground' boundary layer was present. Some

qualitative discussion is then given of the vorticity dynamics associated with this mechanism, and it is shown that, although the flow field is steady, examination of the transient process by which this steady state is achieved is crucial for its interpretation.

2. Experimental facility and technique

2.1. *Modelling considerations*

In order to model the three-dimensional flow field produced by a jet engine operating near the ground, one must adopt some approximations. As one example, Reynolds numbers $V_\infty D/\nu$ observed in practice for a typical high-bypass-ratio engine are on the order of 10^6, based on moderate ambient wind velocity and the inlet diameter. It is thus not practical to keep Reynolds-number similarity. Because of this, the locations of separation lines would be expected to be different from the actual case; this applies as well to the thickness and velocity distribution in the various boundary layers that are present.

It is to be emphasized, however, that the experiments are aimed at presenting a clear qualitative picture of the physical mechanism, rather than obtaining quantitative data in a situation where the basic fluid-dynamical processes are reasonably well defined. The precise location and strength of these separation lines, for example, is not a question that bears strongly on the description of the vortex-formation process given herein. In addition, the emphasis is on the global features of the flow, for example the total circulation around the core, since it is these global parameters that are significant for engine stability. Thus the detailed features of the viscous layers are also of secondary importance.

In summary, the lower Reynolds numbers of the experiments compared with the actual situation mean that there will be quantitative differences in the results in the two cases. However, the overall features of the phenomenon, such as, for example, the question posed in §1.1 about the two legs of the ingested vortex line, should be similar in the two cases, and it is these features that we wish to clarify. On this level, therefore, the model experiments should provide a useful guide for understanding these types of flows. Further comments about this aspect will be given in the discussion of the experimental results.

The essential features of the phenomenon can be seen in an incompressible flow. In the actual situation there are regions where the Mach numbers are near unity, but these only occur very locally near the inlet lip. Further, the nature of the fluid-dynamical device causing the mass flow into the inlet will not affect the process of vortex formation outside the inlet, and hence one does not have to simulate the turbomachinery components.

In this investigation the ambient vorticity that is typically present in the vicinity of an outdoor test stand or an airfield is simulated using a honeycomb of non-uniform length to generate the required velocity profile. The actual ambient vorticity encountered in practice can have two components normal to the mean-flow direction, as well as a streamwise or Beltrami component. In the present investigations we have chosen to examine the effect of the two normal components separately. Hence the velocity-profile generators are designed to create a far-upstream flow in which the vortex lines are normal to the mean flow and *either* perpendicular to the ground plane (vertical) in the one case, or parallel to the ground plane (horizontal) in the other.

Normally the vorticity due to wind shear is relatively weak. It must therefore be substantially amplified (in the neighbourhood of the engine) for an inlet vortex to

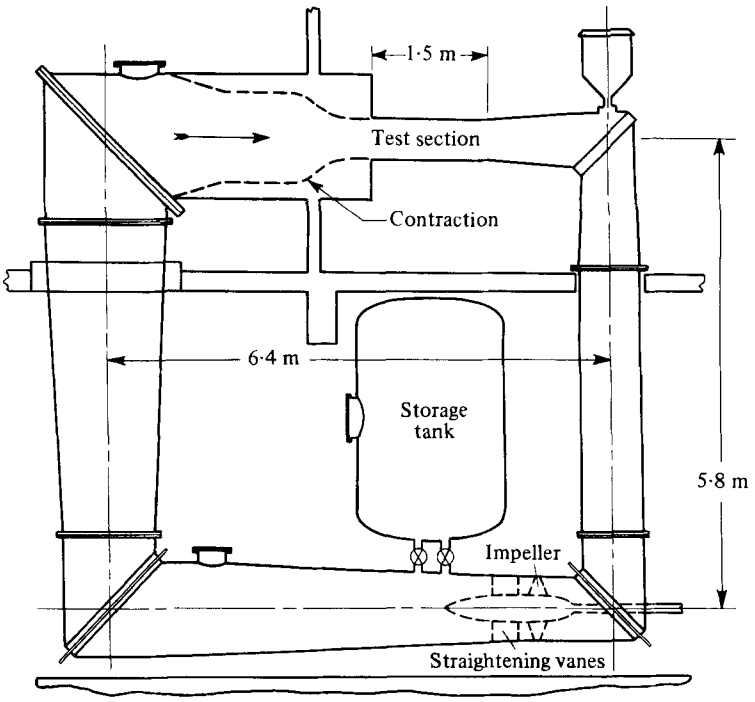

FIGURE 2. M.I.T. Ocean Engineering water tunnel.

form. One objective of this study is to obtain an understanding of the three-dimensional inlet flow field (and vortex formation) between a far-upstream location and the engine inlet. In the water-tunnel investigations of the flows considered, lines of (hydrogen-bubble) fluid markers could be produced that were to a good approximation material lines, and material lines were essentially vortex lines. The changes in vorticity magnitude and direction can thus be discerned by observing the deformation of a line of these bubbles as it is convected downstream and ingested into the inlet. In addition to the tests with a shear flow, in order to determine the role of the ambient vorticity in inlet vortex formation, experiments were also carried out with an upstream irrotational flow.

2.2. *Water-tunnel facility*

The flow-visualization studies were carried out in the 6000 gallon capacity M.I.T. Ocean Engineering Water Tunnel. A schematic of this facility is shown in figure 2. In this investigation, it was run with a free surface. The 1·5 m long, 0·5 m square test section is preceded by a large settling chamber with a honeycomb structure, followed by a contraction, in order to reduce velocity non-uniformities and turbulence level in the tunnel. The resulting flow is of high quality and is well suited for flow-visualization studies.

Downstream of the test section, there is a diffuser and a turning vane section; above this vaned section, a vacuum chamber is positioned. The large storage tank on the lower level of the tunnel permits draining of the test section; it can be refilled in 3–4 min using a 350 gallon per minute pump. A 0·77 m inside diameter impeller (see figure 2) provides the flow through this tunnel. More detailed information is given by Kerwin (1967).

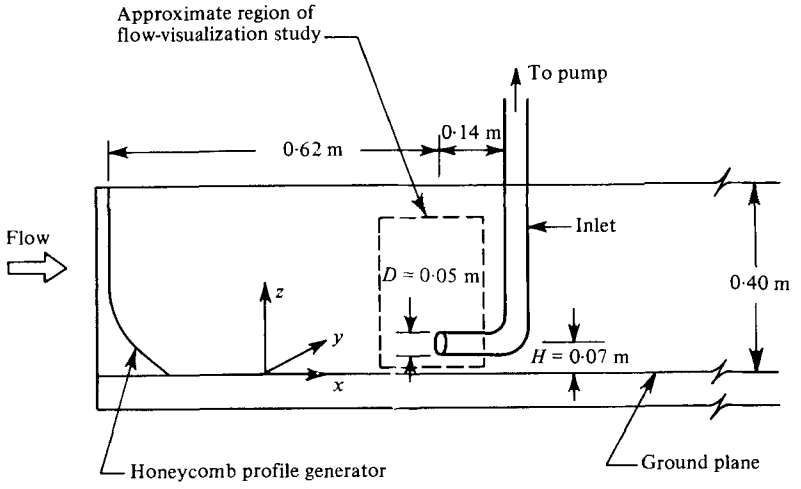

FIGURE 3. Water-tunnel test section; inlet oriented at 0° to the mean flow.

2.3. *Inlet geometries*

The engine inlet is modelled in this investigation using a (Plexiglas) pipe, with the suction provided by a downstream centrifugal pump. Three different inlet configurations were studied in some detail: an inlet near a ground plane at 0° to the far upstream mean flow; an inlet near a ground plane at 90° to the far-upstream flow, i.e. in cross wind, and a *twin-inlet* configuration at 90° to the mean flow. The inside diameters were 0·044 m, 0·05 m and 0·025 m respectively. All three inlets are (platinum) wired for hydrogen-bubble flow visualization in order to determine the location of the vortex in the inlet; the wire is located 0·03 m downstream of the inlet lip and is oriented normal to the inlet axis. The rear of the 0° inlet was constructed out of Plexiglas so that, using a downstream mirror, the location and sense of rotation of the vortex in the inlet could be seen. A sketch of the water-tunnel test section with a 0° inlet configuration is shown in figure 3, which also indicates the coordinate system that we will use to describe the results. The x-coordinate is in the direction of the mean flow, the y-coordinate is normal to the mean flow and in the ground plane (i.e. the ground plane is the (x, y)-plane), and the z-coordinate is normal to the ground plane.

The ratio of the inlet centerline height from the ground plane (or symmetry plane in the case of the twin inlet) to the inlet diameter was held constant at 1·4 for all three configurations. This is a number typical of centerline-height-to-diameter ratios of current gas-turbine engines on wide-body aircraft.

2.4. *Shear-profile generation*

As shown in figure 3, the required velocity profiles were generated using honeycomb of nonuniform lengths, designed according to the calculation procedure of Kotansky (1966). Four different profiles were created: a boundary-layer-type flow, a jet-type flow, a 'clockwise' shear and a 'counterclockwise' shear.

Typical velocity profiles can be seen in figure 4. The profile shown in figure 4(*c*) will be referred to as the *clockwise* shear, and that in figure 4(*d*) as the *counterclockwise* shear. This nomenclature is based on viewing the velocity profiles from *below* the tunnel, i.e. looking in the direction of the positive z-axis. This convention provides

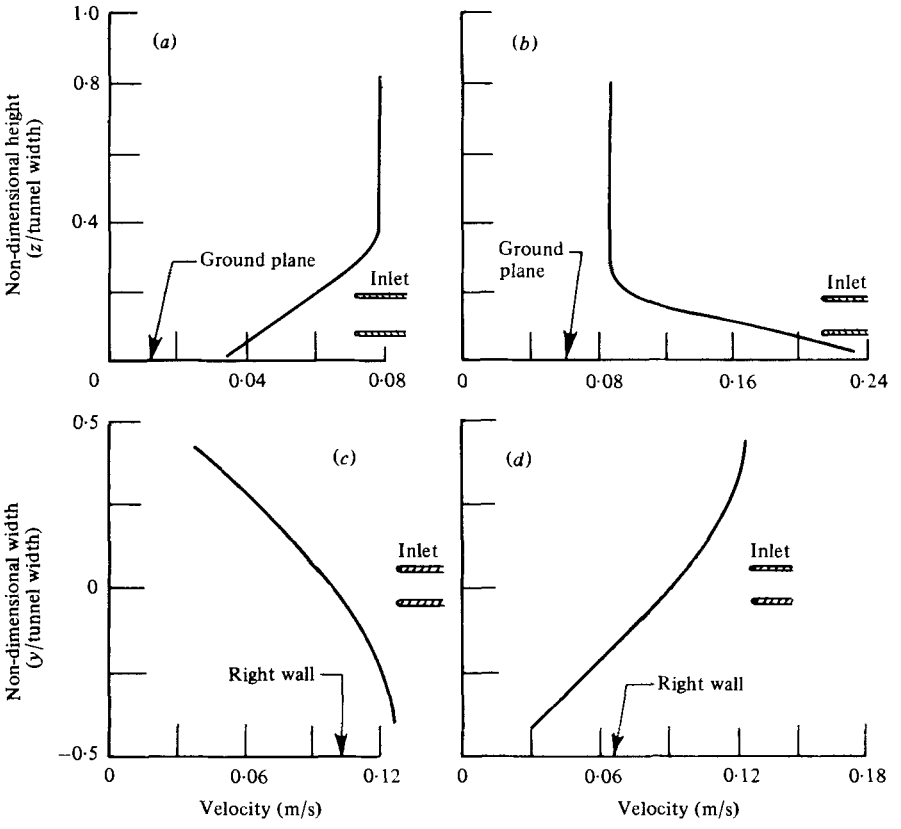

FIGURE 4. Velocity profiles (calculated from hydrogen-bubble flow visualization): (*a*) boundary-layer-type profile; (*b*) jet-type profile; (*c*) clockwise shear profile; (*d*) counterclockwise shear profile.

a more consistent terminology in the discussion of the experimental results.† The velocities have been shown in dimensional form to indicate the actual range of velocities at which the hydrogen bubble technique was used. The vertical axis in the figures is the non-dimensional transverse (y) coordinate, or the non-dimensional height above the ground plane (z-coordinate).

Note that the lengthscales of these shear profiles are far larger than in those associated with viscous diffusion. In the present set of experiments the shear layers were between 0·1 and 0·4 m thick. A representative diffusion lengthscale is of order $(\nu x/U_\infty)^{\frac{1}{2}}$, where x is the distance from the downstream edge of the honeycomb to the inlet. With typical values of $x = 0{\cdot}6$ m and $U_\infty = 0{\cdot}08$ m/s we find $(\nu x/U_\infty)^{\frac{1}{2}} \approx 0{\cdot}003$ m. Thus, although viscous effects (in the honeycomb) are crucial in creating the shear layer, they can be expected to play only a small role as the fluid is ingested into the inlet because of the relatively short distance over which the inlet influences the flow appreciably, *except* in regions of high vortex stretching, or in the boundary layers. This is also true in the actual situation, where non-uniform velocities can be created over an upstream length that is several orders of magnitude larger than the inlet height.

† Note that the profiles shown in Figure 4 (*c*, *d*) are plotted in the usual manner, i.e. as viewed from above the tunnel.

The two velocity profiles shown in figure 4(*a*, *b*) have vortex lines that are, far upstream of the inlet, parallel to the ground plane and normal to the mean flow, i.e. parallel to the y-axis. For the 'boundary-layer-type' profile the sense of the rotation is clockwise when viewed from the 90° position (looking along the y-axis from negative to positive). For the jet-type profile the sense of rotation is counterclockwise when viewed from the same vantage point. (Since the flow satisfies the no-slip condition, it is clear that there must be a thin viscous region with clockwise rotation below the region with counterclockwise rotation. However, the thickness of the former is an order of magnitude smaller than the thickness of the latter.)

The two velocity profiles in figure 4(*c*, *d*) have vortex lines that, far upstream, are along the z-axis, i.e. perpendicular to the ground plane, and to the mean-flow direction.† These represent velocity gradients that might result from a wind that varied in magnitude from one location to another in the same horizontal plane.

2.5. *Flow-visualization technique*

Hydrogen-bubble generation was used for the flow-visualization method. In this technique, which is described in detail by Clutter, Smith & Brazier (1959), by Schraub *et al.* (1964), and by Mattingly (1966), a thin platinum wire is employed as the cathode of a d.c. circuit for electrolysis. Small hydrogen bubbles (of diameter on the order of the wire diameter) are formed at this cathode and swept off by hydrodynamic forces. For the range of velocities and wire sizes used in this study the bubbles follow the flow very well and give an excellent indication of the fluid motion (Schraub *et al.* 1964). In addition to bubble wires embedded in the inlet, three different wire probes (with wire diameter of 0·025 mm) were used to examine the flow: a 0·30 m vertical wire, a 0·23 m horizontal wire, and a smaller probe, which could be inserted at various positions in the flow field. Details of the probes and lighting are given by De Siervi (1981).

2.6. *Experimental procedure*

Prior to the starting of a series of runs, the water tunnel was de-aerated for several hours. The tunnel velocity and the inlet velocity were then set to the desired reading. Since each honeycomb shape had a different resistance, the tunnel velocity was calibrated separately for each shape by taking photographs of hydrogen bubbles generated at a known frequency.

The flow around the single inlet was investigated for each of the four shear profiles at 0° and 90° of yaw. In addition to the above two orientations, the single inlet and twin inlet in irrotational flow were also studied at 270° of yaw to check overall tunnel flow symmetry. The transient conditions involved in the inlet vortex start-up and cessation, for the single- and twin-inlet configurations oriented at 90° to the main upstream flow, were examined by decreasing the tunnel velocity while keeping the velocity V_i in the inlet constant at 1·2 m/s, as well as by keeping the tunnel velocity V_∞ constant at 0·08 m/s and decreasing the flow through the inlet.

The hydrogen bubbles were photographed and were also videotaped, the latter procedure being far more suitable in the present experiments since the water tunnel was in high demand. Since the videotape pictures cannot be reproduced photographically with the desired resolution, drawings based on (lengthy) observation of the actual phenomenon and of these videotapes will form the backbone of the experimental observations that are reported.

† Again, this cannot be true in the thin groundplane boundary layer because of the no-slip condition (Lighthill 1963). However, we will still use this manner of reference in discussing these particular velocity profiles.

3. Inlet-vortex formation due to intensification of ambient vorticity: experiments and analysis for an inlet at 0° of yaw

3.1. *Experimental results*

As stated, we have chosen to present and discuss the experimental results in two parts to illustrate separately the central features of the two mechanisms that we have mentioned. In this section therefore we consider the situation with an inlet at 0° of yaw. The ambient velocity profiles examined were an irrotational (outside of the thin ground-plane boundary layer) flow, a boundary-layer-type shear (see figure 4*a*), and the clockwise and counterclockwise shears (see figures 4*c*, *d*).

At ratios of V_i/V_∞ that are of interest for this phenomenon (i.e. > 5, say), for the 'irrotational' case two small counterrotating vortices appeared, symmetrically placed about the 6:00 (six o'clock) position. These are associated with the ground-plane boundary layer and this test thus served as a check on the general symmetry and uniformity of the tunnel flow.

As expected, an essentially symmetric picture was also seen for the case of the boundary-layer-type shear profile (horizontal vortex lines). Two (approximately) equal (in size) but opposite (in sense) vortices were again found. These were located in the lower half of the inlet at roughly the 5:30 and 6:30 positions.† Owing to the increased extent of the rotational region in the upstream flow, the vortices were considerably larger than those due just to the natural (viscous) boundary layer. Observations of the behaviour of material lines show that, as might be expected in this symmetric configuration, the centre of the material line is ingested into the inlet first, with the two vortices resulting from this stretching of initially parallel vortex filaments. De Siervi (1981) gives further details of the behaviour of material lines (i.e. vortex lines) at different heights above the ground plane.

The results with an upstream flow having vortex lines that were initially vertical, i.e. perpendicular to the ground plane, were quite different. At the velocity ratio examined in detail, $V_i/V_\infty = 10$, a *single*, steady vortex was present in the inlet at approximately 6:00 and roughly 0·8 inlet centreline heights from the ground plane. The leg of the vortex that was in front of the inlet was associated with a large-scale spiralling flow extending between the ground plane and the inlet. The diameter of the spiral was roughly one-third of the inlet diameter and decreased as one moved towards the inlet. Hydrogen bubbles introduced into the centre of the spiral appeared as a thin thread stretching almost vertically into the inlet from the ground plane.

The position and scale of the vortex in the inlet can be seen in figure 5, which is a photograph taken looking into the inlet. The arrow points to the vortex, as indicated by the hydrogen bubbles, which show up as bright areas. The sense of rotation is the way in which one would see it looking into the inlet from upstream. The light 'spokes' seen in the figures are the roughly radial bubble wires (and the associated bubble production). The very bright regions on the top and bottom of the inlet and the annular light region are due to reflections associated with the Plexiglas tube; these could not be avoided with the experimental configuration that was used.

In this configuration the sense of rotation of the vortex was determined solely by the sense of the ambient vorticity. Thus the clockwise and counterclockwise shears (figures 4(*c*, *d*), which were created by reversing the same piece of non-uniform honeycomb) gave rise to flows which were very similar, except that the sense of rotation of the vortex was reversed. For the clockwise shear (clockwise rotation

† The use of the 'clock' nomenclature is a convenient way to describe position in the inlet. All of the positions described are in the sense of an observer looking *into the inlet from upstream*.

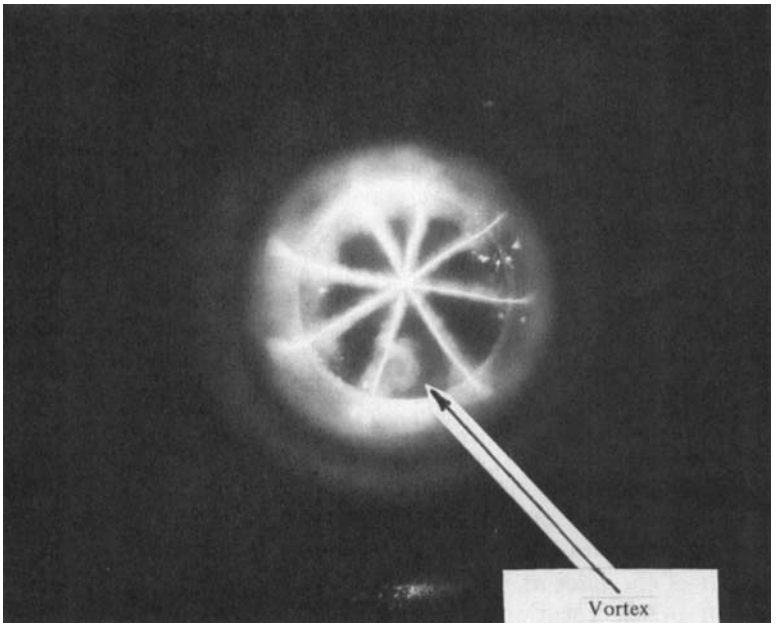

FIGURE 5. Ingestion of a vertical vortex line (clockwise shear) into a 0° inlet; view looking upstream through a mirror (photograph of hydrogen-bubble flow visualization).

looking *up* at the tunnel) the inlet vortex had a clockwise rotation as seen looking into the inlet from upstream. For the counterclockwise shear the rotation was counterclockwise. These directions are consistent with those obtained if one considers vortex lines extending from locations on the ground plane in front of the inlet lip to the lower half of the inlet. It thus seems that the appearance of an inlet vortex is associated with the stretching of (ambient) vertical vortex lines in the region below the inlet lip. The basic question about the existence of the other leg of the vortex lines, which was posed in §1.1, still remains, however. To resolve this, as well as to understand the process of vortex formation better, let us now examine the vorticity field in the region of the inlet.

3.2. *A secondary-flow approach to the vorticity field*

We consider an incompressible, constant-density, inviscid flow with no body forces. In this situation the vortex filaments are always composed of the same fluid particles. For a given vortex filament, the ratio of the vorticity to the length of the filament remains constant, so, if a vortex filament is stretched, the vorticity associated with it increases.

To calculate the evolution of vortex filaments as they move toward the engine requires the determination of the velocity field. The flow under consideration is clearly rotational, not only in a thin layer as in many aerodynamic applications but throughout the flow domain, and is also strongly three-dimensional. However, since the basic concept to be studied is the intensification of vorticity due to the stretching of the vortex filaments as they are drawn into the inlet, a useful simplification can be made by viewing the problem as a 'small-shear, large-disturbance flow', as described by Hawthorne (1967). In this approximation the flow is assumed to be composed of an irrotational primary flow and a superposed weak shear flow. The vortex filaments associated with this shear are regarded as being deformed by this

primary flow only, i.e. the influence of the so-called 'secondary' velocities on the convection of vortex filaments is neglected. The primary flow can be determined using potential-flow theory and advantage can be taken of the fact that many numerical methods now exist to compute potential flows around complex geometries.

The secondary-flow approximation can be stated explicitly as follows. We assume that the three-dimensional velocity field can be written as

$$\mathbf{V}(x, y, z) = \mathbf{V}_0(x, y, z) + \mathbf{v}_1(x, y, z). \tag{1}$$

$\mathbf{V}_0$ represents the primary flow and $\mathbf{v}_1$ the secondary flow, both of which are three-dimensional. The magnitude of $\mathbf{v}_1$ is taken to be such that a linearized description of the *secondary flow field* can be adopted. The primary flow is irrotational, and all vorticity is thus associated with the secondary flow field only:

$$\boldsymbol{\omega} = \boldsymbol{\omega}_1 = \nabla \times \mathbf{v}_1. \tag{2}$$

The secondary-flow approximation is equivalent to a linearization of the vorticity equation, which can thus be written as

$$(\mathbf{V}_0 . \nabla)\, \boldsymbol{\omega}_1 = (\boldsymbol{\omega}_1 . \nabla)\, \mathbf{V}_0. \tag{3}$$

It can be seen that terms that are quadratic in the '1' quantities, and which represent the convection and distortion of the secondary vorticity field by the secondary velocity field, have been neglected. Even though (3) is linear in the secondary vorticity $\boldsymbol{\omega}_1$, $\mathbf{V}_0$ is a fully three-dimensional function of position (known numerically), so that one can describe the process of vorticity amplification due to vortex-line stretching, which is an important feature of inlet vortex formation.

The equation expressing the variation of vorticity of a fluid particle can be cast into a simpler form. If we denote distance along the primary-flow streamlines by S_0, (3) can be written as

$$\frac{\partial \boldsymbol{\omega}_1}{\partial S_0} = \frac{1}{|V_0|} (\boldsymbol{\omega}_1 . \nabla)\, \mathbf{V}_0. \tag{4}$$

Knowing the primary-flow streamlines and velocity distribution, (4) could, in principle, be integrated along a streamline to find the change in vorticity for a given fluid particle.

The above formulation is the way in which the secondary-flow approximation is often presented. In the present application, however, it is more convenient to track fluid particles, obtaining changes in the vorticity directly from changes in the length and orientation of specified fluid elements. If $\delta\mathbf{l}(t_A)$ is the length of an infinitesimal material line element that coincides with a vortex line at an initial time t_A, the vorticity at time t is related to that at t_A by

$$\frac{\boldsymbol{\omega}_1(t)}{|\boldsymbol{\omega}_1(t_A)|} = \frac{\delta\mathbf{l}(t)}{|\delta\mathbf{l}(t_A)|}. \tag{5}$$

In (5) the quantity $\delta\mathbf{l}(t)/|\delta\mathbf{l}t_A)|$ is, within the context of the secondary-flow approximation, a function of the primary-flow velocity field only.†

† This could also be viewed as a simple application of the Cauchy equation for the vorticity (Batchelor 1967), which in the present situation takes the form

$$\boldsymbol{\omega}_1(t) = \omega_{1i}(t_A) \frac{\partial \boldsymbol{X}}{\partial a_i}.$$

Here $\mathbf{a}$ and $\mathbf{X}(\mathbf{a}, t)$ are the position vectors of one end of the material line element at times t_A and t respectively, and the tensor $\partial\mathbf{X}/\partial a_i$ is a function of the known primary flow, which can be evaluated numerically.

In following the motion of selected particles and/or material lines it is helpful to use the 'drift', or displacement of fluid particles (Lighthill 1956) as the quantity that is studied. In steady flow streamlines and pathlines coincide, and, in such a case, the trajectory of any particle can be readily deduced from an integration along the streamlines. Further, the manner in which a given particle describes its trajectory can be determined from the drift-time concept. The drift time T for a fluid particle to travel between locations 1 and 2 on a streamline can be defined as

$$T = \int_1^2 \frac{dS}{V}, \tag{6}$$

where dS is distance along a streamline and V is the magnitude of the velocity.

In a steady flow, for any given streamline this quantity depends only on the end points. Since points on a given material line or surface will have the same drift times, one can follow (numerically) a particular material line on surface as it is convected by the primary flow. The deformation of given vortex lines, and hence the strength and orientation of the vorticity can thus be computed.

As a last note of background on the secondary-flow approach, we can point out that the approximations inherent in the theory will not hold where nonlinear and/or viscous effects are important, e.g. where there is intense vortex stretching or very near stagnation points where the primary velocity becomes small. However, what is of interest is the global behaviour, and, as in the experiments, the details of the flow *in* the regions mentioned above are of less concern at present than their integral properties. The approach taken is suitable for examining the latter.

The steps used in calculating the vorticity field were as follows. Firstly, an inlet/ground-plane geometry was selected and the previously introduced overall parameters describing the inlet vortex formation given typical values. Secondly, the three-dimensional potential flow about the inlet was determined numerically. Thirdly, selected vortex lines (material lines) were tracked (numerically) from far upstream to the inlet. From the stretching and 'tipping' they undergo we can predict the vorticity pattern at the engine face, given a far-upstream vorticity distribution. A further step, as described by Viguier (1980), would then consist of computing the secondary velocity field produced at this location by the calculated vorticity distribution.

The far-upstream (ambient) vorticity can be resolved into three components: (i) x-component (streamwise); (ii) y-component, transverse to the flow direction and parallel to the ground plane (horizontal); and (iii) z-component, transverse to the flow direction and normal to the ground plane (vertical). The evolution of the streamwise component can be predicted very simply and will hence be only briefly discussed.

Consider a flow that has, at a far-upstream location, streamwise vorticity only. For a constant-density inviscid flow with conservative body forces, the vorticity everywhere downstream will also be in the streamwise direction, and the strength of the streamwise vorticity at any location is directly proportional to the velocity. The ratio of the streamwise vorticity at the engine face location to that far upstream is therefore just equal to V_i/V_∞. The flow situations we are concerned with are characterized by large values of this parameter, say 10 or greater, and the streamwise vorticity can be expected to increase by an order of magnitude or more between far upstream and the compressor face.

In spite of this, however, this process does *not* appear to be the primary cause of inlet-vortex formation. The inlet-vortex formation described in the literature depends strongly on the angle of yaw of the inlet; whereas the mechanism just described is independent of it. In addition, in the inlet-vortex experiments described herein, the

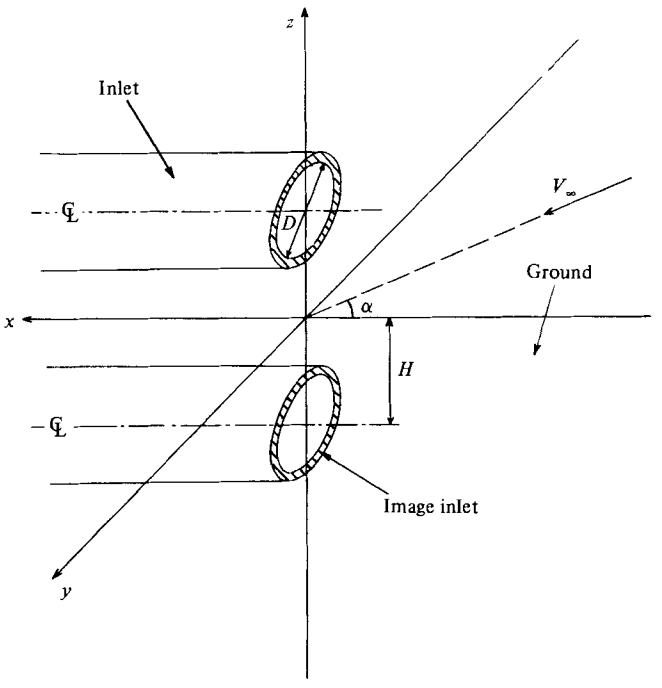

FIGURE 6. Geometry for potential-flow calculation.

shear was generated by a honeycomb, so no component of streamwise vorticity existed far upstream. Further, the situation that one generally finds in an engine test is some sort of shear layer associated with a boundary layer, or wake; so that the flow consists essentially of normal vorticity at the far-upstream location. Last, but perhaps strongest, the inherently three-dimensional process that leads to stretching of vortex filaments that were initially normal to the streamlines appears to be considerably more potent than the essentially one-dimensional effect described above. Estimates of the latter, in fact, imply that it is far too weak to give rise to the strong vortices that are actually seen. Thus the focus here is on the components of vorticity that are *normal* to the streamlines at the far upstream location.

3.3. *Flow geometry used in the analysis*

The specific flow geometry that is analysed can be seen in figure 6. It consists of a cylindrical inlet (without centre body) and its image, which is introduced to simulate the ground plane. For the general situation the inlets are set at a yaw angle α in a uniform stream, with direction parallel to the plane of symmetry between the inlet and its image and magnitude V_∞. In the case to be discussed at present, α is zero. The operating condition for a given inlet at a given H/D (height-to-diameter ratio) is thus defined by a single non-dimensional parameter: the ratio V_i/V_∞ of inlet velocity to far upstream velocity.

3.4. *Three-dimensional potential-flow calculation procedure*

The approach taken requires the potential flow about the geometry described above to be computed. Many different methods exist to calculate potential flow about three-dimensional bodies. It is not within the scope of this paper to describe them in detail, and a complete coverage of these matters can be found in the abundant literature (e.g. Hess & Smith 1966; Hess 1972, 1974; Rubbert 1978; Johnson 1980).

The computational method used in the present study was the constant-strength source and dipole method developed by Hess, Mack & Stockman (1979) specifically for the flow about three-dimensional inlets. In this method a general solution to the problem is composed of four fundamental solutions, which can be combined linearly to give the flow about the inlet at various operating conditions. The fundamental solutions consist of the flows induced by unit-value onset flows parallel to the three coordinate axes as well as the flow through the inlet in static operation. The last of these, which is of primary importance in the situations that we are concerned with, is produced by a distribution of unit vortices on the inlet surface. (Actually a doublet distribution is employed and use is made of the relationship between the derivatives of doublet strength and vorticity given by Hess (1972).) These vortices are placed in such a way that they form vortex rings, which, for an axisymmetric inlet geometry, are oriented exactly on the circular cross-sections.

A description of the program, as well as a more thorough presentation of the method, is given by Hess *et al.* (1979). The computational method requires a large amount of storage, and this put a limitation on the number of panels that could be utilized to describe the inlet. Based on initial numerical experiments in which we varied the number and circumferential positioning of the panels, the calculations were carried out using 240 (planar quadrilateral) panels and eleven 'N-lines' on each half inlet.

Once the fundamental solutions are determined, the primary flow about the inlet at any operating condition can be studied. We chose to investigate an inlet with velocity ratio V_i/V_∞ of 30 and an H/D of 1·25. At this velocity ratio the static solution was the largest contribution to the flow field. This, combined with the storage limitation mentioned above, meant that there was a region of (re)circulating flow adjacent to the inlet and that the stagnation points did not occur on the outer surface of the inlet, but off the inlet. In a sense, then, this gave us an inlet configuration that had an 'effective' shape with a much thicker lip and a somewhat different external geometry than that specified by the input geometry. In addition, since the space between the inlet and the ground is filled with recirculating flow, the inlet external surface is seen by the oncoming flow as extending to the ground plane. Because of this recirculation, some aspects of the flow field cannot be described adequately using the present computational method, although others can be seen clearly. This distinction between what can and cannot be resolved with an analysis of the present type will be given in more detail in what follows.

3.5. *Behaviour of the material lines*

The behaviour of selected material lines has been examined to show the convection and amplification of the vortex filaments. As discussed previously, the far-upstream vorticity can be resolved into three components. Since we are interested in those situations in which a single inlet vortex exists, based on the experimental results we examine here the behaviour of vortex lines that are vertical far upstream. Based on results of the potential-flow computations, a location four inlet-centreline heights upstream of the inlet face was used as the starting point of these material-line drift calculations.

Figure 7 shows the subsequent shapes of a vortex line that is (initially) vertical far upstream and is on the plane of symmetry, i.e. the (x, y)-plane. The vortex line is shown at different times, and it can be seen that this filament undergoes substantial stretching as it enters the inlet. This stretching appears to be relatively symmetric in spite of the fact that there is a stagnation streamline, shown as a dash–dot line, on the lower side of the inlet only. The projection of the capture surface (defined here

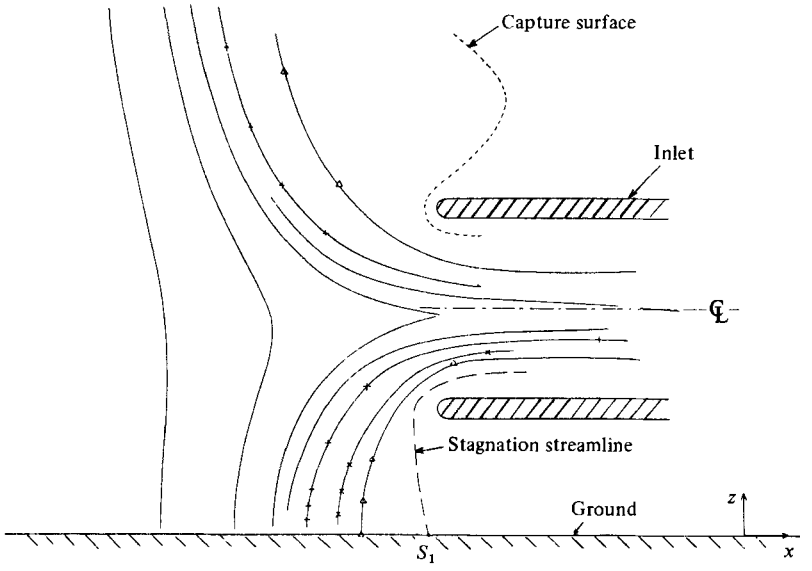

FIGURE 7. Deformation of a material line (vortex line) that is vertical and in the (x, z)-plane at a location four inlet heights upstream of inlet; inlet at zero yaw.

as the surface separating flow that enters the inlet for the first time from flow that does not enter, or re-enters the inlet (owing to recirculation)) on the (x, y)-plane is also shown in figure 7 as a dashed line, to give an indication of the extent of the recirculation region.

More interesting behaviour, however, is exhibited by vortex filaments off the plane of symmetry. Figures 8 and 9 show two different views of a vortex line that is vertical far upstream and 0·60 inlet heights (0·75 inlet diameters) from the (x, z)-plane. Figure 8 shows the projections on the (x, z)-plane, with the numbers corresponding to different times. The situation appears quite similar to that occurring *on* the (x, z)-plane as regards top and bottom symmetry. However, figure 9 shows the projections of this same filament on a plane normal to the inlet axis (i.e. on the (y, z)-plane). It can be seen that, from this view, there is distinct difference between top and bottom sections. This is associated with the existence of the stagnation point on the ground. In particular, the lower part of the filament at the latest time illustrated ('9') has drifted considerably closer to the midplane of the inlet (in fact, to the location of the stagnation streamline) than has the upper part.

This tendency is shown even more clearly in figure 10, which shows projections, on the same plane, of the positions of a vortex line that is near the capture surface far upstream, being initially at 1·6 inlet heights (2·0 inlet diameters) from the (x, z)-plane. Note that, since vortex lines cannot end in the flow, the lines tracked in this figure, as well as those in figures 7–9, actually extend to infinity. However, those portions of the material lines *outside* the capture surface, which do not enter the inlet, are not shown.

Both the 'head' (top) and the 'foot' (bottom) of the sections of material lines that are shown will lag behind the middle, since particles that are on the ground plane will stay there, while particles near the capture surface will not only have a larger path to travel than particles interior to this surface but have also lower velocities. The result is, as shown by the computation, that the two 'legs' of the vortex line are both strongly stretched and consequently have high vorticity levels. Quantitative

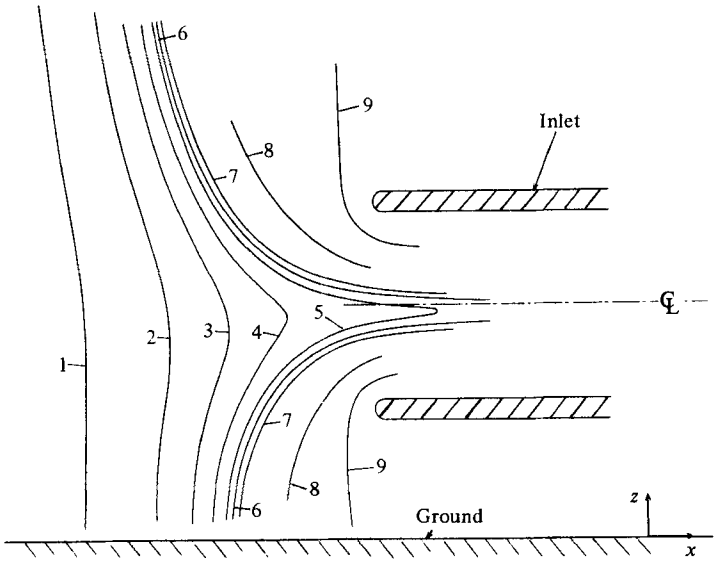

FIGURE 8. Deformation of a material line (vortex line) that is initially vertical and 0·6 inlet heights from the (x, z)-plane at a location four inlet heights upstream of inlet; projections on (x, z)-plane; inlet at zero yaw.

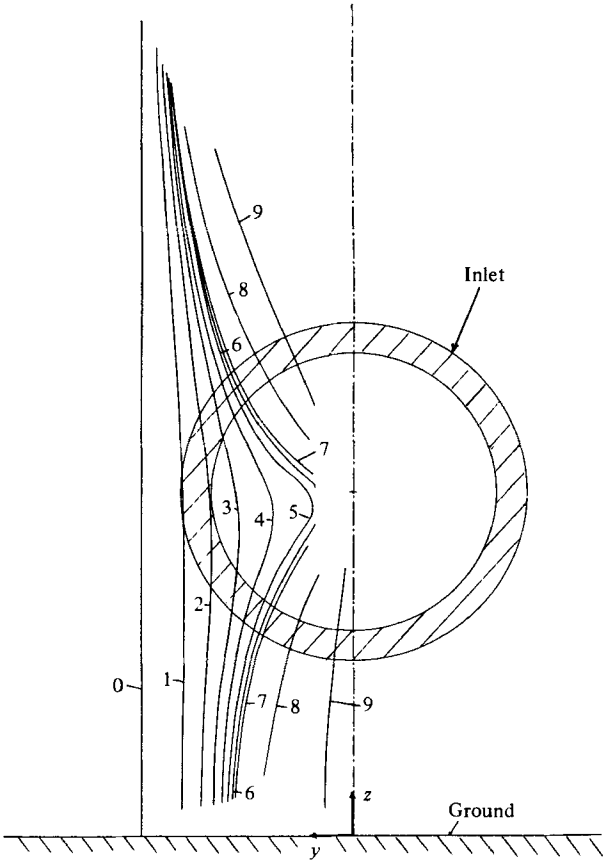

FIGURE 9. Projections of material lines shown in figure 8 on (y, z)-plane.

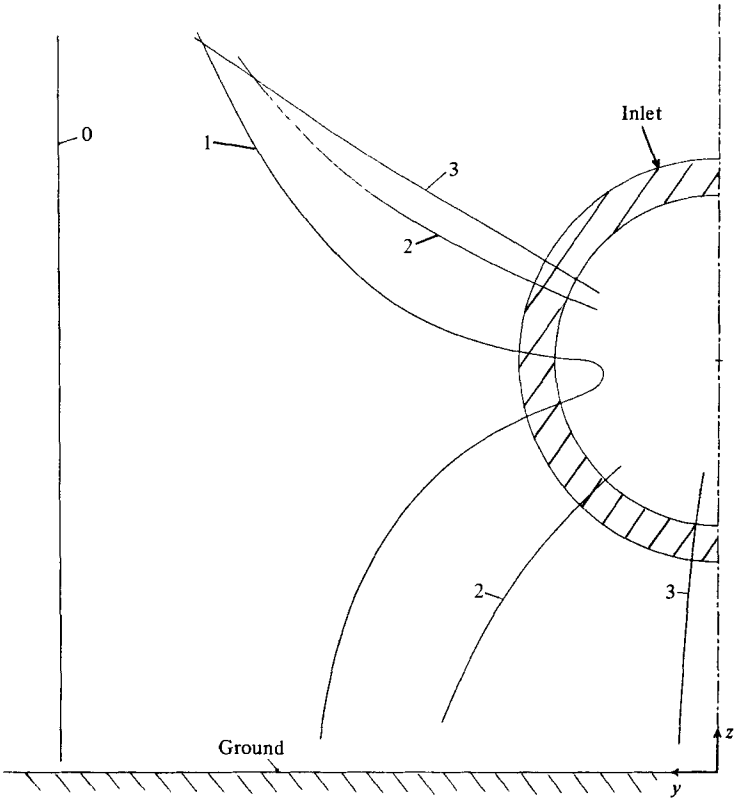

FIGURE 10. Deformations of a material line that is vertical and 1·6 inlet heights from the (x, z)-plane at a location four inlet heights upstream of the inlet; projections on the (y, z)-plane; inlet at zero yaw.

appreciation of this stretching, however, is difficult from only the tracking of material lines, since the deformation increases rapidly for fluid particles close to the ground plane or the capture surface. A conceptual scheme for calculating the vorticity levels of both legs and the corresponding secondary velocity is given by Viguier (1980).

3.6. *Concentration of vortex lines and inlet-vortex formation*

The study of the deformations of material lines initially off the $(x. y)$-plane gives a strong hint of a possible inlet-vortex formation mechanism. As stated, the existence of two stretched legs and the observation of a single vortex seem difficult to reconcile. However, the locations of these legs must also be examined. The foot of any vortex line will approach the ground-plane stagnation point in front of the inlet, with the associated lower leg approaching the stagnation streamline. In contrast, the location reached by the upper leg, which extends from the inlet up to the vortex-line 'head' (defined as the top of that part of the vortex line which is inside of the capture surface) depends on the vortex-line *initial position*. To a good approximation the computations show that the streamline followed by a fluid particle that coincides with the head of a vortex line will lie in a plane through the inlet centreline and the capture surface.

Using this information, we can thus determine the ultimate position of the vortex line head, and figure 11, which is based on the extensive computations that have been carried out, shows the suggested deformation of vertical material lines within the capture surface. A far-upstream uniform distribution of vertical vortex lines evolves

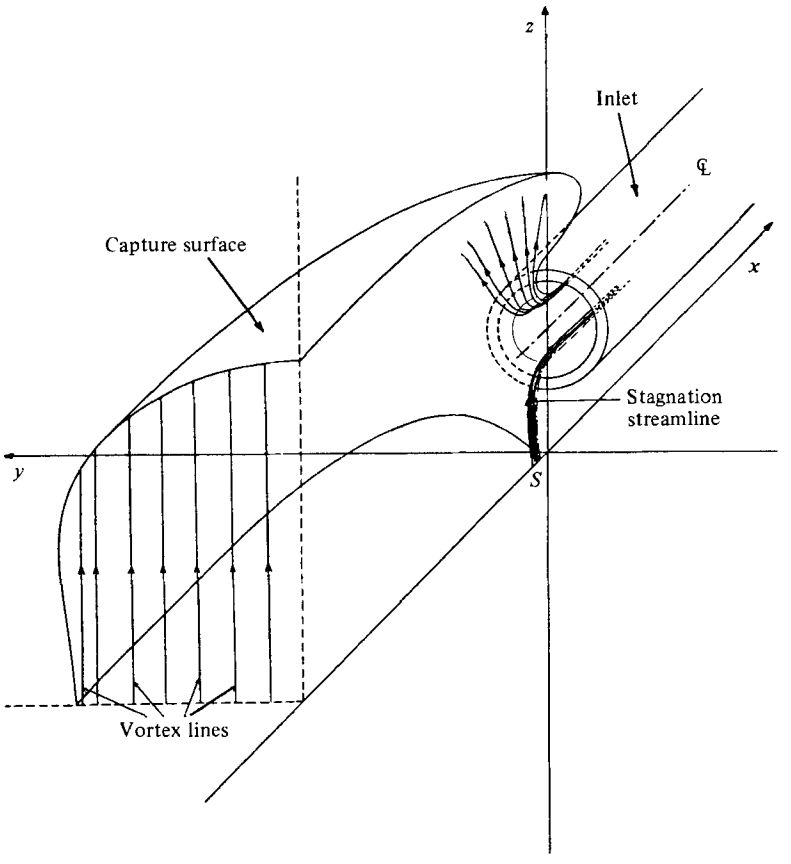

FIGURE 11. Suggested deformation of a far-upstream uniform distribution of vertical vortex lines.

into a configuration in which the upper legs of the lines are 'fanned out' over the upper part of the inlet while the lower legs are concentrated around the stagnation streamline associated with the stagnation point S, in the figure. (Again, for clarity only portions of the upper legs of the vortex lines have been shown.) Although the stagnation point is never reached in an actual flow, the basic phenomenon of this concentration of vortex lines will still occur. The predicted concentration is accompanied by an increase of the associated circulation per unit area. Note that in the calculation, in which all viscous effects are neglected, the eventual stretching of both legs will be infinite. There is an important difference, however, in the spatial distribution of the vorticity amplification.

To state this another way, the computations show that one can, to a good approximation, regard the behaviour of the lower and upper parts of the ingested vortex lines as that associated with three-dimensional stagnation-point flow versus two-dimensional stagnation-line flow respectively. The former leads to a much higher concentration of vorticity than the latter owing to the lower parts of the vortex lines being 'gathered' together (round the stagnation streamline), as well as stretched, while the upper portions are stretched only.

Upstream flow	Time dependence
Single inlet	
Irrotational flow	Steady and transient
Boundary layer, horizontal vortex lines (figure 4*a*)	Steady
Jet, horizontal vortex lines (figure 4*b*)	Steady
Clockwise† shear, vertical vortex lines (figure 4*c*)	Steady
Counterclockwise† shear, vertical vortex lines (figure 4*d*)	Steady
Twin inlets	
Irrotational flow	Steady and transient

† As observed from below.

TABLE 1

4. Experiments with an inlet at 90° of yaw

The mechanism described above should come into play whenever there is a vertical component of vorticity, whatever the angle α at which the upstream flow approaches the inlet. With a non-zero yaw angle, however, there is a second basic mechanism that can give rise to the formation of an inlet vortex. This could be seen in experiments that were carried out with a cylindrical inlet having an axis at 90° to the upstream flow. The specific configurations examined are listed in table 1.

As a preliminary to the experiments, it is useful to describe briefly some further results of the secondary-flow calculations, which were carried out with an inlet at a non-zero yaw angle. As discussed by Viguier (1980), owing to storage limitations we could not examine an inlet at 90°. The calculations were thus done at a yaw angle of 45°, but the central qualitative conclusions should still be applicable. It was found that the vorticity field due to vertical vortex filaments possesses many of the features seen in the 0° yaw case, with a strong concentration of vortex lines about the stagnation streamline, and a fanning out of the vortex lines in the upper half of the inlet. Thus this case really yields no additional features of the phenomenon to those discussed previously.

The drift of horizontal vortex lines was also examined to see if any concentration of vortex lines would occur owing to the asymmetry of the flow. The calculations showed, however, that there did not appear to be any situation of this kind. To see this we can examine one representative situation: a horizontal vortex line that is, far upstream, 0·4 inlet heights from the ground plane. Other filaments at both larger and smaller heights showed substantially the same behaviour.

Figure 12 shows the projections of the positions of this vortex line on the (y, z)-plane (the plane perpendicular to the inlet axis). As before, only the part inside the capture surface is shown. The fluid particles on the vortex line close to the capture surface are seen to lag behind, while those in the middle (of the portion that is shown) enter the engine much sooner. The corresponding legs are observed to be rather symmetrically placed, however, and both legs of the vortex lines are strongly stretched. Thus no clear indication of a definite vortex due to ingestion of far-upstream horizontal vortex lines can be seen from the present calculation.

4.1. *Experiments with the boundary-layer-type velocity profile*

Based on the calculations, it might be expected that the ingestion of horizontal vortex lines into a 90° oriented inlet would result in two asymmetrically placed

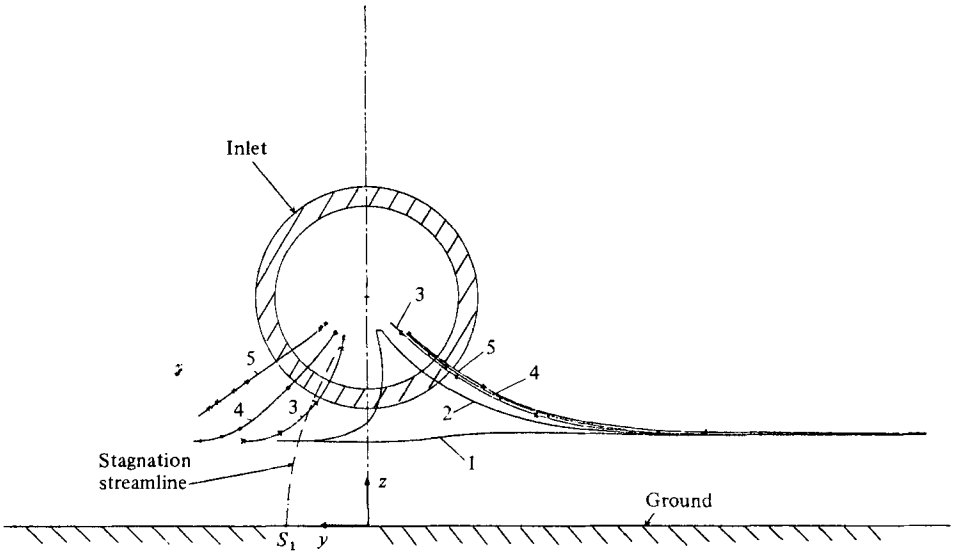

FIGURE 12. Deformations of a material line that is initially horizontal and 0·4 inlet heights from the ground plane; projections on the (y, z)-plane; inlet at 45° of yaw.

counterrotating vortices, but no predominant single concentration of vorticity. The circulation around the two legs would be of the same magnitude, although the vorticity would not necessarily be equal. The actual situation, however, is quite different. This can be seen in figure 13, which is drawn from (prolonged) observation of the hydrogen bubbles (De Siervi, 1981). In these observations, material lines were examined that originated at different heights above the ground plane. Figure 13 shows the convection of a horizontal fluid line originating at roughly 0·1 inlet centreline heights above the ground plane. The velocity ratio is approximately 10.

It can be seen that a central section is drawn into the inlet first with the two 'ends' entering at a later time. The vortex lines enter the inlet at roughly the same height and with the opposite sense of rotation. However, the flow pattern is asymmetric and the strength of the two vortices appears to be quite different.

The *clockwise* vortex (as viewed looking into the inlet) encompasses a larger proportion of the inlet area and also appears to rotate faster. This leg stems from the separation region located underneath the inlet and 0·8–0·9 inlet-centreline heights from the inlet lip. It is associated with a large clockwise spiralling flow extending between the ground plane and the inlet in the region directly in front and on the right half of the inlet. The diameter of this spiral decreases as it approaches the inlet. A hydrogen-bubble-marked thread of fluid particles could be seen to extend vertically up through the centre of the spiral and into the inlet. Outside of the inlet, this clockwise spiral encircled the counterclockwise vortex leg. At this velocity ratio, if the vortex line were initially higher than roughly 0·6 inlet-centreline heights, the clockwise leg was ingested without being caught in the outside spiral. It is apparent that the secondary-flow approach does not describe this situation.

4.2. *Experiments with the jet-type profile*

The jet profile (figure 4*b*) required substantially higher velocity ratios (roughly 40) for a vortex to form than with the boundary-layer-type profile. Consequently the usefulness of the flow-visualization probes was limited (because of wire breakage) and

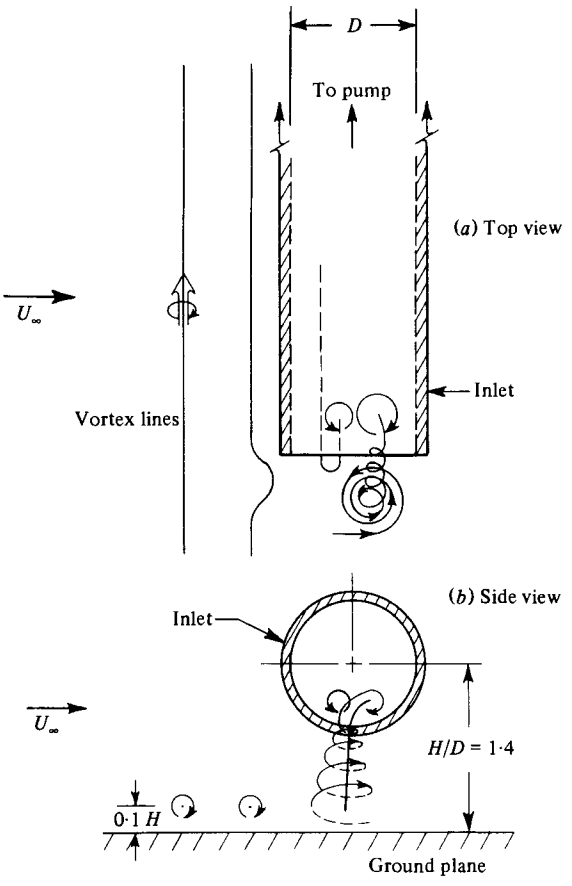

FIGURE 13. Ingestion of horizontal vortex lines originating at $0{\cdot}1H$ into an inlet at 90° of yaw (drawn from hydrogen-bubble flow-visualization results).

only a small amount of data was obtained. For this 90° inlet configuration, the ingestion of initially horizontal vortex lines possessing rotation with a counterclockwise sense resulted in the formation of a single clockwise-rotating vortex.

4.3 *Experiments with clockwise and counterclockwise shears*

For an inlet oriented at 90° to the mean upstream flow, the presence of far-upstream vertical vorticity with clockwise rotation (when viewed looking up at the tunnel) resulted in a single clockwise vortex inside the inlet. This observation can perhaps be expected in view of the discussion of the secondary-flow results. However, with far-upstream vertical vorticity having counterclockwise rotation, a single clockwise vortex inside the inlet was also found. The sense of rotation of the vortex is thus opposite to the ambient vorticity and this would not occur if the only mechanism were the amplification of ambient vorticity. This is another indication that there is a clockwise 'bias' in the circulation of the vortex created when the inlet is oriented at 90° to the mean flow, and that a mechanism other than the stretching and intensification of far-upstream vorticity is responsible.

5. Experiments with an inlet in irrotational flow: a description of a new mechanism for inlet-vortex formation

The presence of the clockwise-rotation bias exhibited in the 90° inlet configuration motivated further examination of the inlet flow field with an irrotational upstream flow. To carry out this study the tunnel was run with no added resistances. The upstream flow was thus uniform, aside from the thin (displacement thickness estimated to be approximately 5 mm) boundary layers on the walls and floor of the tunnel. The flow outside of the boundary layer possessed no swirl, as far as could be seen.

As stated previously, two small, roughly equal and opposite, vortices associated with the floor boundary layer, had been found when the inlet was at 0°. This indicates that the overall flow in the tunnel in that situation was quite symmetric. The clockwise bias found when the inlet is at 90° is thus not from an asymmetry due to the tunnel but rather due to the inherent asymmetry present in the flow around the inlet.

In other words, in some of the situations in which we created a shear flow far upstream, the inlet vortex was found to rotate in the opposite direction from that expected using basic arguments about the stretching of ambient vortex lines. Thus, *another mechanism* must be operating. If this does not depend on ambient shear, it should be observable in a uniform flow. A caveat is that the 'other mechanism' might have been some gross asymmetry in the tunnel; however, the test referred to above indicates that no such large departure from symmetry exists. It is to be emphasized that the departure from non-uniformity that was looked for *must* be a large one and should be readily visible, since the ambient shear used in the first set of experiments was reasonably strong.

5.1. *Inlet at 90° of yaw in an irrotational flow*

With this configuration a strong steady vortex was observed in the lower part of the inlet at approximately the 6:00 location. The size and location of the vortex can be seen in figure 14. This photograph shows the hydrogen bubbles shed from the wires in the inlet (as in figure 5, these are seen as the bright 'spokes' in figure 14). The velocity ratio V_i/V_∞ was approximately 20. The sense of the rotation was clockwise when viewed looking into the inlet.

Further examination of the flow field revealed another important feature. This was a *trailing vortex*, from the downstream side (outside) of the inlet lip region. The relative position and size of this trailing vortex, compared with the inlet vortex, is shown in figure 15, which is based on observations of the hydrogen-bubble flow visualization. The trailing vortex is considerably larger than the inlet vortex, with the diameter of the apparent vortical region being roughly 0·9 inlet diameters. The sense of rotation was clockwise, viewed from upstream.

A schematic of the pattern of vortex lines implied by this flow is presented in figure 16. This shows the sense of rotation of the inlet and trailing vortices and also indicates the vortex lines that thread through the ground boundary layer into the inlet vortex (Lighthill 1963).

The reason for the trailing vortex can be seen from consideration of the circulation round the inlet. Let us compare the circulation round a contour enclosing the inlet and far away the lip (curve C_1 in figure 17) with that round a contour that encloses the vortex and is near the inlet lip (curve C_2 in figure 17). Several diameters from the lip, the flow round the inlet should be roughly two-dimensional, and the velocities

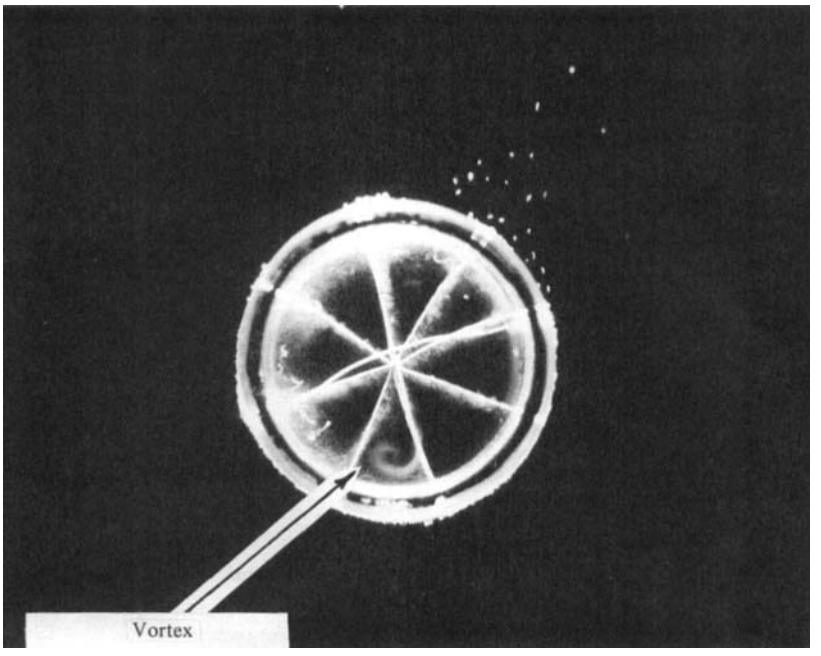

FIGURE 14. Inlet vortex in an inlet at 90° of yaw in an irrotational upstream flow.

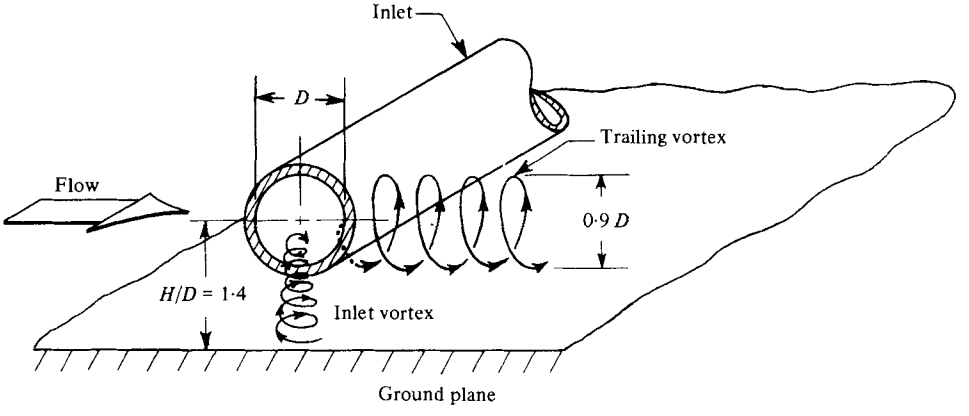

FIGURE 15. Streamlines associated with inlet at 90° of yaw in an irrotational upstream flow (drawn from hydrogen-bubble flow visualization).

on the order of the velocity V_∞ at infinity. The circulation around the inlet at C_1 should therefore scale as $V_\infty D$.

From data on the flow around a two-dimensional cylinder/ground-plane configuration (Bearman & Zdravkovich 1978), one can very crudely estimate the constant of proportionality in this scaling to be roughly $\frac{1}{7}$. The circulation should thus be small compared with $V_\infty D$ for locations on the inlet that are far from the lip. However, consider now the circulation round the inlet vortex. The velocities associated with the vortex are an order of magnitude larger than V_∞ (they are of the order of the inlet velocity) and the lengthscale is a significant fraction of the inlet diameter. The circulation round the inlet vortex is thus estimated to be more than an order of magnitude greater than the circulation round the cylindrical inlet at a station far from the lip.

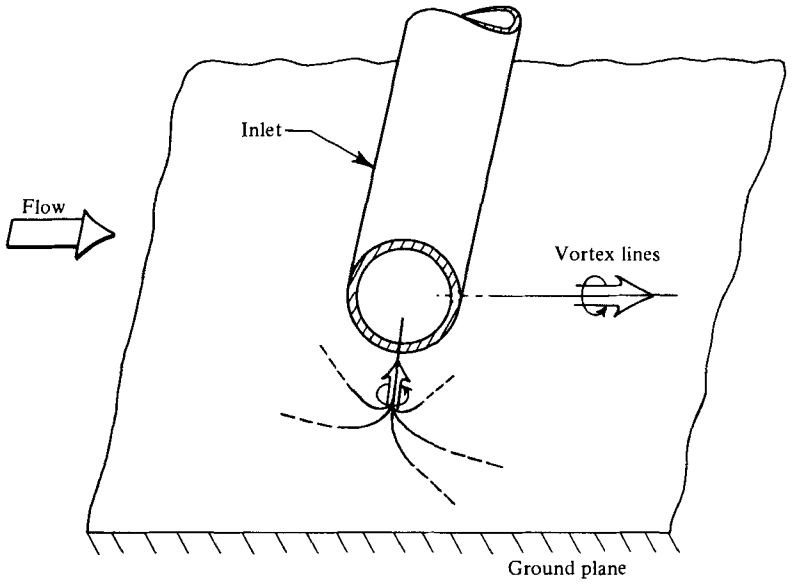

FIGURE 16. Schematic vortex lines for an inlet at 90° of yaw in an irrotational upstream flow.

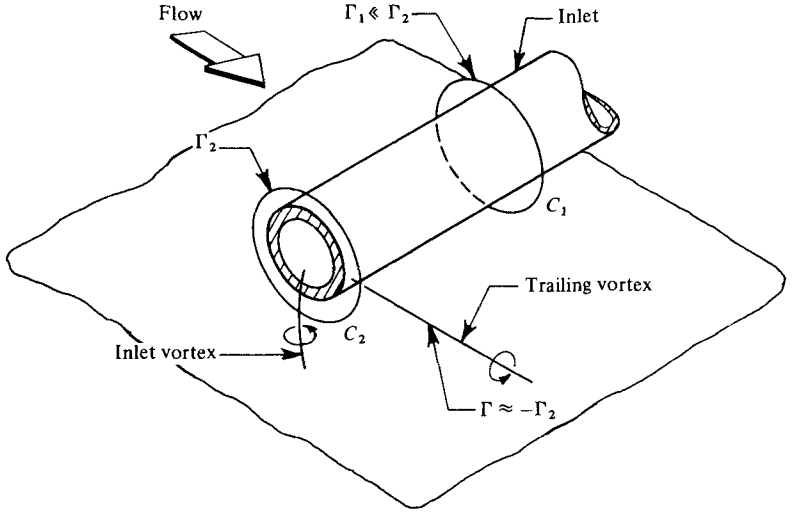

FIGURE 17. Variation of circulation along the length of an inlet at 90° of yaw in an irrotational upstream flow.

The situation is thus as shown in figure 17. The circulation round contour C_1 at the distant location is small relative to that round contour C_2 outside the lip. This latter contour includes the inlet vortex, and the circulation round it may in fact be close to that round the inlet vortex. Because of the difference in circulation, there must be trailing vorticity between the two contours, as is indicated in the figure. An inlet with only a single vortex is not possible, since there would then be a large net circulation round the inlet at any station along the inlet, and this is incompatible with the conditions that occur at locations far from the inlet lip. To restate the argument in a slightly different manner, we can say that there is no mechanism to

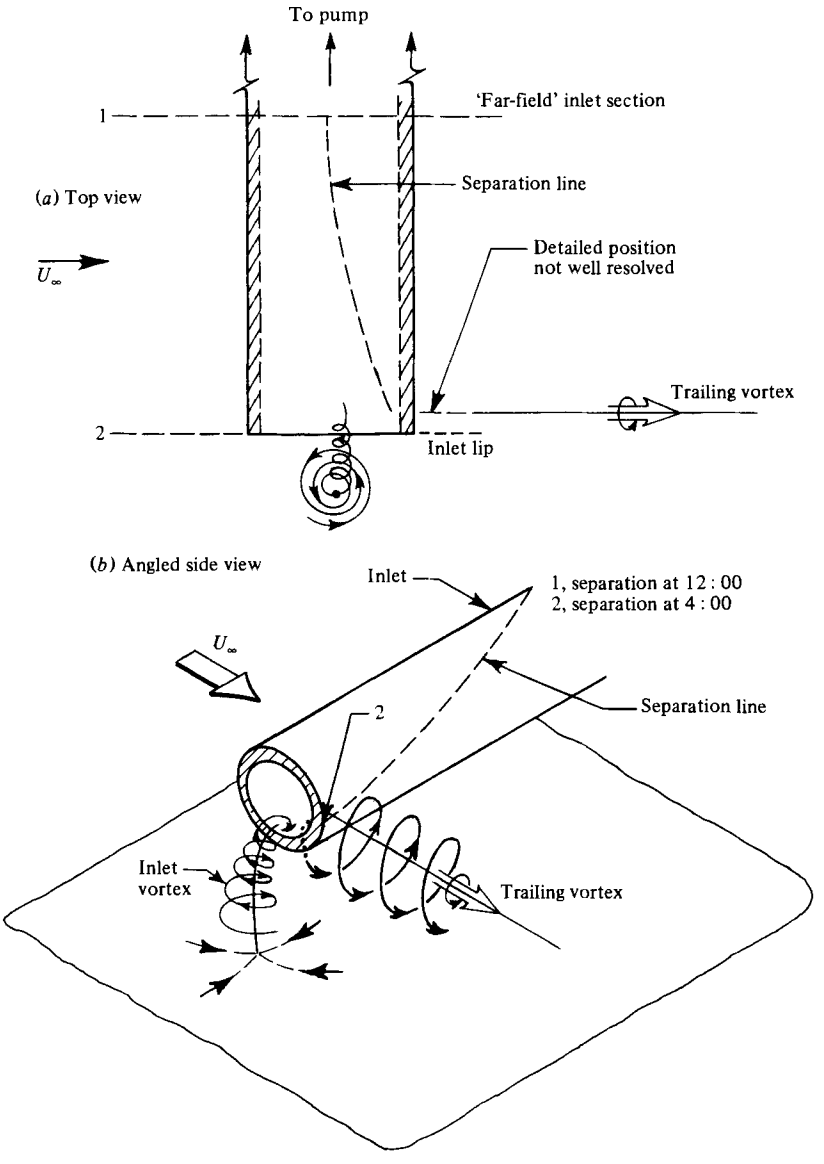

FIGURE 18. Variation of upper-separation-point location along the axial length of an inlet at 90° of yaw in an irrotational upstream flow (drawn from hydrogen-bubble flow visualization): (*a*) top view; (*b*) angled side view.

cause an appreciable circulation round the inlet at a location far from the lip. Thus the presence of a (ground-plane-to-)inlet vortex requires the presence of a trailing vortex (or vortices) with a circulation of comparable magnitude.

We can thus see that with an upstream irrotational flow the inlet vortex is part of a vortex system. An analogy exists, in fact, between this system and that (half of) the vortex system of a finite wing; this will be brought out further when we discuss the twin-inlet results. In both types of flow it is the spatial variation of circulation that is responsible for the trailing vortex.

The change in circulation along the length of the inlet could be observed with the

flow-visualization technique by examining the separation of the flow as it passed over (and under) the inlet. The change in circulation was associated with a skew in the separation line, which appears qualitatively as shown in figures 18(*a*,*b*) (drawn from the observations). At station 1, which is far from the inlet lip, the flow separated at approximately 12:00 and 6:00, with the dividing streamline impinging on the inlet at 9:00. This near symmetry implies that there is near-zero circulation at this station, similar to the two-dimensional results for a cylinder near a ground plane at the present H/D value (Bearman & Zdravkovich 1978).

Proceeding along the inlet (parallel to the axis) towards the inlet lip (station 2) one finds an increasing asymmetry in the separation locations. The separation location on the upper surface moves further in the clockwise direction than the one on the lower surface moves in the counterclockwise direction, so that at station 2 the separation locations are roughly at 4:00 and 6:00. In addition, as one approaches the lip, the velocity increases. The combination of the shift in the position of separation and the increase in the velocity as one nears the lip imply a substantial (clockwise) circulation around the inlet in the neighbourhood of the lip. Presumably the asymmetric flow separation and the clockwise circulation are both due to the non-symmetric pressure field resulting from the ground-plane–cylinder interaction at high values of V_i/V_∞. However, whatever the detailed mechanism, it is clear that the variation of circulation along the inlet is directly linked to the generation of the trailing-vortex system, and thus to the inlet-vortex formation.

It is also of interest to examine the changes in flow regime encountered as V_i/V_∞ is increased. At low, but non-zero, values of V_i/V_∞ (say < 5 for the present configuration) the capture streamlines do not touch the ground, there is no stagnation point on the ground and no inlet vortex. Separation from the rear of the inlet lip is nearly symmetric and occurs near the 3:00 location. As shown in figure 19(*a*) (which is sketched from the flow visualization results) there are *two* counter-rotating vortices, of roughly equal strength, that trail from the rear of the inlet. The view in the figure is directly into the inlet, i.e. normal to V_∞.

As the velocity ratio is increased, the separation location shifts in the clockwise direction and the upper trailing vortex becomes relatively stronger than the lower. This shift could be seen clearly in the videotapes, which the authors would be pleased to lend to interested readers. Further increases in V_i/V_∞ cause the disappearance of the lower trailing vortex and the formation of a (ground-plane-to-)inlet vortex, as indicated in figure 19(*b*). In summary, the movement of the inlet lip separation points, and the formation of the inlet-vortex–trailing-vortex system are interrelated and dependent on the ratio V_i/V_∞ of tunnel velocity to inlet velocity. For low V_i/V_∞ no inlet vortex exists, and two counter-rotating trailing vortices are present, but as V_i/V_∞ increases the flow field evolves into an inlet-vortex–single-trailing-vortex configuration.

5.2. *Experiments with twin inlets: the role of the ground boundary layer*

We have focused so far on the overall features of the inlet-vortex system. Another question concerns the role of the ground boundary layer. It is true that the ground boundary layer *can* be the source of the vorticity that must exist in the core of the inlet vortex, and which is convected along the axis of the vortex into the inlet. However, the overall features of the velocity field outside of the viscous regions might not be expected to be greatly dependent on the characteristics of this ground boundary layer, or even, perhaps, on whether there *is* a ground boundary layer.

To investigate this, we examined a twin-inlet configuration (one above the other)

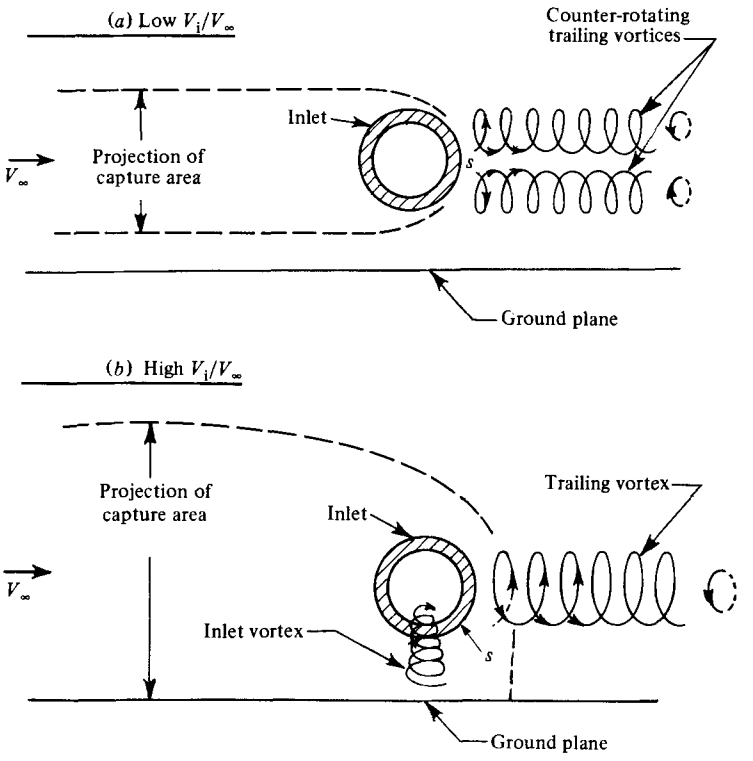

FIGURE 19. Flow regimes at 'low' (e.g. $\leqslant 5$) and 'high' (e.g. $\geqslant 20$) values of V_i/V_∞. Inlet at 90° of yaw in an irrotational upstream flow (S denotes approximate location of region of separation at rear of inlet): (*a*) low V_i/V_∞; (*b*) high V_i/V_∞.

in an irrotational flow (figure 20). The inlets were tested at 90° as well as at 270° angle of yaw (i.e. facing in the opposite direction). They were located at the centre of the tunnel far from the walls. The centerline 'height' to diameter ratio for *each* inlet was 1·4 (i.e. the centre-to-centre distance was 2·8), as with the single inlet. The inlets were geometrically identical and the (downstream) resistance characteristics of each were made high enough so that the flow would have a plane of symmetry between them at the same geometrical position as the ground plane. Flow visualization showed that the streamlines were indeed quite symmetrical with respect to this plane. The replacement of the ground plane, and its boundary layer, by this (inviscid) plane of symmetry thus allows us to study inlet-vortex formation with no ambient vorticity upstream of the inlet.

The investiation of the twin-inlet configuration at 90° of yaw revealed a steady, strong, clockwise (when viewed looking up at the tunnel) vortex, which stretched between the two inlets. A trailing vortex was evident from the outside of each of the inlets. The inlet vortex entered the top (bottom) inlet at approximately 6:00 (12:00), with a clockwise (counterclockwise) sense of rotation when viewed looking into the inlet. The centre of the vortex core was at times quite apparent owing to cavitation along its length.

The streamlines for this configuration were as sketched in figure 21, which also shows the relative scale of the trailing vortex and of the vortex between the inlets. The overall flow field for *each* inlet was thus similar to that for the single-inlet situation. A schematic of the vortex lines for the flow past twin inlets is shown in figure 22. It can be seen that there is indeed an overall analogy with the vortex system

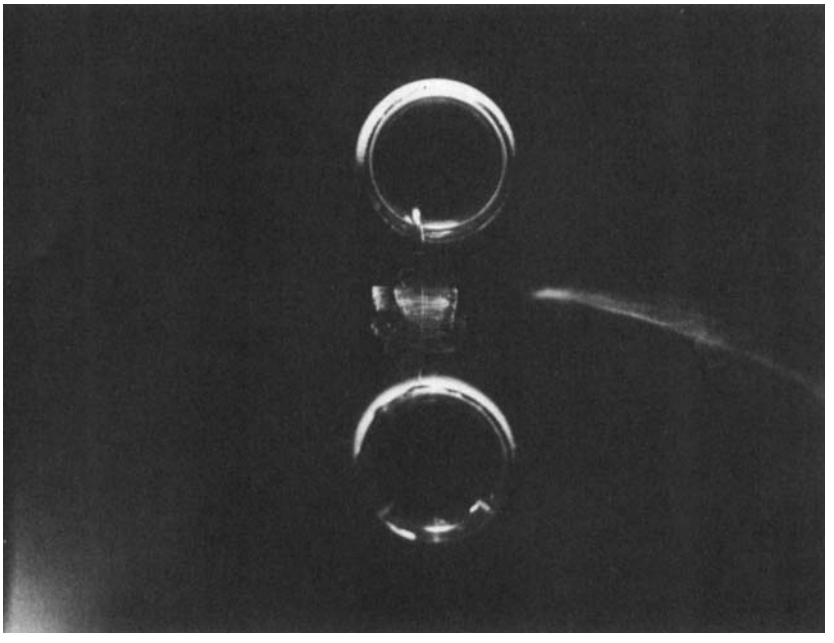

FIGURE 20. Vortex core extending between twin inlets at 90° of yaw in an irrotational upstream flow (photograph of hydrogen-bubble flow visualization).

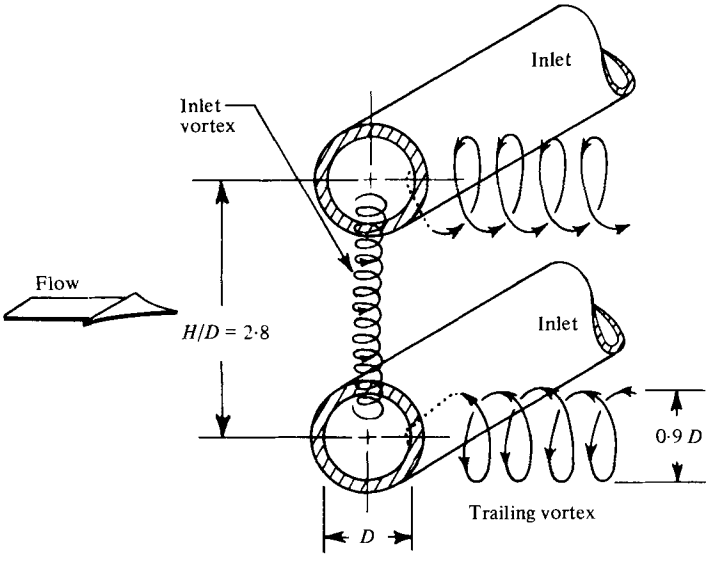

FIGURE 21. Streamlines associated with twin inlets at 90° of yaw in an irrotational upstream flow (drawn from hydrogen-bubble flow visualization).

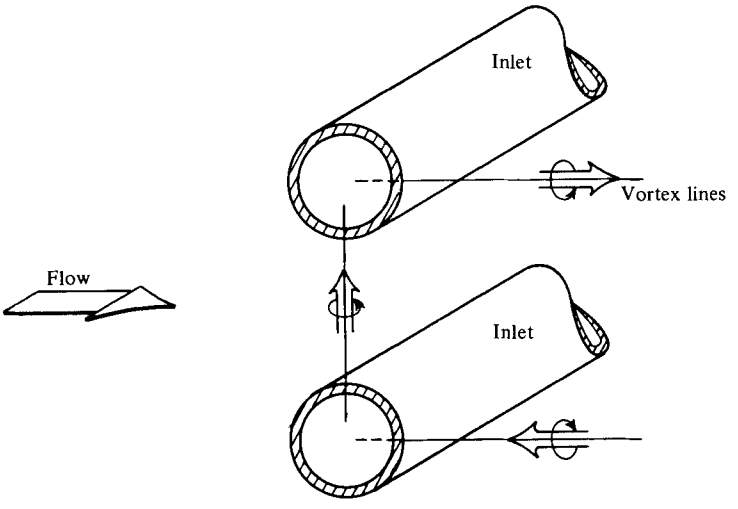

FIGURE 22. Schematic of vortex lines for twin inlets at 90° of yaw in an irrotational upstream flow.

of a finite wing, although, as discussed below, the details of the processes responsible for the generation and maintenance of the vorticity in the core that stretches between the inlets are quite different from those occurring in the case of the wing. The circulation around the inlet was found to vary with axial distance from the inlet lip, as in the single-inlet configuration.

Tests were also carried out with the twin inlets facing the opposite way (i.e. at 270° of yaw). A reversed, but otherwise similar, vortex system was found, again indicating that the phenomenon is not due to ambient vorticity, but rather to the asymmetry produced by the inlet flow.

In examining the twin-inlet configuration, a further question arose concerning the source of the vorticity in the vortex core between the inlets. Specifically, the flow visualization showed that at steady-state conditions there was no flow of vortical fluid into this vortex from the boundary layers on the inlets. The vortex cores were thus surrounded only by (irrotational) fluid that had come from upstream. In the cores, however, there is a continual convection of vorticity along the axis away from the symmetry plane and into both inlets (the flow along the axis could readily be seen with the hydrogen bubbles). Thus one can inquire how the vorticity in the core is maintained in the light of this convection, as well as what the mechanism is by which it initially appeared.

In order to answer this, as suggested by Marble (1981 personal communication), the inlet configuration was investigated under transient conditions. These consisted simply of turning the pump on or off. In both these cases the final value of pump flow, although *not* the steady-state flow pattern around the inlet, was established in a time of approximately a second, which is a time comparable to, but somewhat longer than, the timescale H/V_∞, for convection past the neighbourhood of the inlet with the free-stream velocity V_∞ (for the double inlets $H/V_\infty \approx 0{\cdot}5$–1 s, depending on the precise conditions). However, the flow visualization showed that the vortex formation occurred mostly after the pump start-up, with the flow achieving a steady state in a time of the order of $10\,H/V$.

In this set of experiments there is no *ambient vorticity* and no ground boundary layer. The vorticity is only created by viscous effects, and the source of the vorticity in the

core must therefore be the boundary layer on the outside of the inlet (i.e. of the Plexiglas pipe). The observations showed that the vorticity comes from this outside surface during the formation process only.

The flow visualization showed that the vortex core started to form just downstream of the inlets, and then strengthened and moved to a position between the inlets as the steady state was approached. The large time needed to form the vortex completely may be due to the time required for the fluid in the boundary layer to be shed into the wake region and then for this slow moving fluid to be convected back upstream. When the flow through the inlet was *stopped*, the process was much more rapid, the vortex detaching from between the inlets and bursting in the region just downstream of the inlets in a time of roughly several H/V_∞.

It is emphasized that once a steady state is attained there is no further convection of vorticity into the core from surrounding fluid. The convection of vorticity out of the region between the inlets (and into the inlets) must thus be balanced by a production of vorticity in this region, due to the stretching of the vortex filaments in the core.

The process can be looked at in several ways. From a local standpoint it can be regarded as a balance between the effects of viscosity, which tends to diffuse the vorticity, and of convection, which tends to inhibit the growth of the regions of rotational flow. In a steady state, the two must be in balance. It is also useful, however, to examine the process from a more global viewpoint. Consider a cylindrical control volume τ surrounding the inlet vortex, as shown in figure 23. An expression for the rate of change of vorticity within this *fixed* control volume τ is derived in the appendix. This is

$$\frac{\partial}{\partial t}\int_\tau \boldsymbol{\omega}\, d\tau = \underset{\text{(I)}}{\int_\tau (\boldsymbol{\omega}\,.\,\nabla)\mathbf{V}\, d\tau} - \underset{\text{(II)}}{\int_s (\hat{\mathbf{n}}\,.\,\mathbf{V})\,\boldsymbol{\omega}\, ds} - \underset{\text{(III)}}{\nu\int_s \hat{\mathbf{n}}\times(\nabla\times\boldsymbol{\omega})\, ds}, \tag{7}$$

where s is the fixed surface bounding τ, and $\hat{\mathbf{n}}$ is the normal to s. The three terms on the right-hand side represent (I) the production of vorticity within the volume, (II) the convection of vorticity out of the volume, and (III) the diffusion of vorticity out of the volume. If we take the radius of the control volume to be large enough so that viscous effects are negligible on the curved sides, then, in a steady state, there is a balance between convection out through the top and bottom, diffusion across the top and bottom surfaces, and production within the volume.

If we examine the order of magnitude of the terms in the integrals on the right-hand side of (7) we find that the ratio of the third term (III) to the first (I) is

$$\frac{\nu\omega_{\text{av}}}{R}\,\pi R^2 \Big/ \frac{V\omega_{\text{av}}}{L}\,\pi R^2 H,$$

where ω_{av} is an average value of the vorticity in the core, L is the relevant lengthscale over which the vorticity varies in the direction along the vortex axis, V is a representative velocity in this direction and R is the radius of the core. If we substitute H for L and V_∞ for V (this latter is most likely an underestimate) as rough estimates of the terms, this ratio becomes ν/RV_∞, which is between 10^{-2} and 10^{-3} for the present set of experiments. Thus the balance is essentially between the production of vorticity within the volume and the convection of vorticity out of the volume. A related illustrative example of this type of balance is given in the appendix, where (7) is applied to the simple case of an infinite vortex strained linearly along

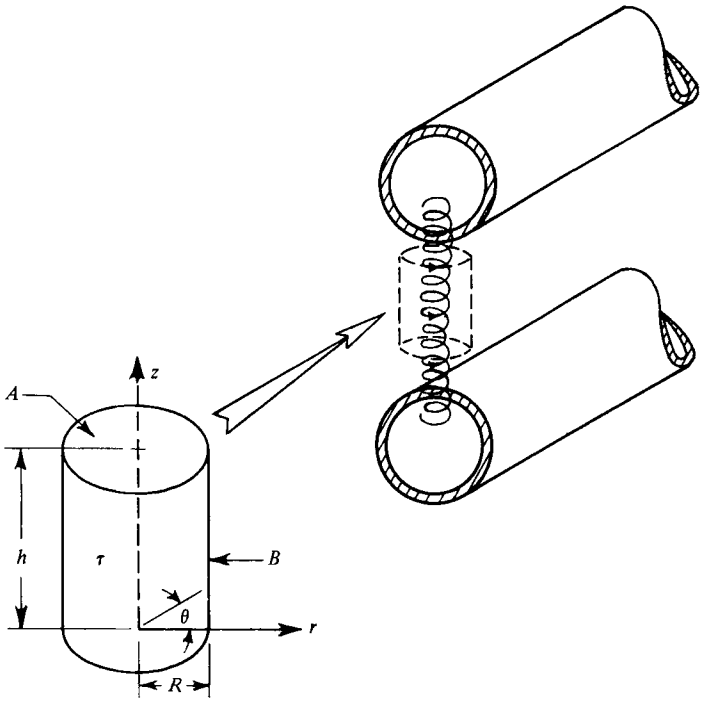

FIGURE 23. Cylindrical control volume around vortex core for twin-inlet configuration.

its axis. In that situation, an exact solution to the Navier–Stokes equations exists, so that the form of the different terms can be specified explicitly.

We summarize the content of the preceding several paragraphs. In this second mechanism of vortex formation, ambient vorticity does not play a role. The vorticity in the core of the vortices is produced initially by the action of viscosity in the boundary layers on the outer surfaces of the inlet. Once the vortex is formed, however, there is no longer any vorticity convected into the core; the vorticity needed to maintain it is produced by the extension of the vortex filaments in the core. Thus the presence of a ground boundary layer (or ambient vorticity) is not necessary for the formation of an inlet vortex.

6. Discussion

In the preceding we have presented two different mechanisms for inlet vortex formation. The first of these, the intensification of ambient (i.e. far-upstream) vertical vorticity, is essentially an inviscid phenomenon, with the role of viscosity being primarily to limit vorticity amplification in regions of high rates of stretching. It thus appears that many of the overall features of this type of flow may be able to be predicted using an inviscid calculation procedure, perhaps coupled with an approximate description of the effects of viscosity.

In the second mechanism the appearance of an inlet vortex is linked directly to the variation in circulation along the length of the inlet. Viscous effects are much more central in creating this type of flow, since the circulation distribution round the inlet is determined by the separation of the three-dimensional boundary layers on the outer surface of the inlet. In most practical inlets there are no salient edges that set these separation points as there are in flow past a wing, flat plate, etc., at an angle of attack.

Finding the circulation therefore involves a calculation of the three-dimensional pressure field round the inlet, as well as of the locations of the boundary-layer separation lines. This is complicated, since in the situation of interest there can be a strong interaction between the viscous and inviscid parts of the flow field.

Although carrying out this type of calculation is beyond the scope of this study, some general comments can be made that address the questions raised in §2.1. First, the experiments were carried out at cylinder Reynolds numbers, based on mean tunnel velocity and inlet outer diameter, of 6000 or less. Consequently the flow around the inlets can be taken to be subcritical (this is also indicated by the wake width and location of the separation points in regions far from the lip). For an actual wide-bodied-aircraft engine inlet in cross-wind the Reynolds number, assuming a wind velocity of 4 m/s and an inlet outer diameter of 3 m, is 8×10^5, which puts it above the value for transition to the supercritical regime, based on a two-dimensional single cylinder. In this regime the upper and lower separation points are closer together than in the subcritical regime. The potential for movement of these points, and hence changes in circulation, may thus be less for the actual inlets than in our experiments.

Secondly, based on the ideas about the two mechanisms, we can attempt to reconcile the various observations that have been made. It should be clear that for an inlet at zero yaw it is the first mechanism, amplification of ambient vertical vorticity, that is responsible for the inlet vortex. On the other hand, for an inlet in an irrotational cross wind it is only the second mechanism, the axial variation of circulation round the inlet, that is relevant. For the cross-wind experiments with shear, however, both mechanisms are interacting. It is an oversimplification to say that the two effects are additive, but one might expect that when the two mechanisms are competing there would be less tendency to form a vortex than when the two are complementing each other. Experiments to examine this interaction between the two mechanisms were not carried out, and we will only comment that in the particular cross-wind cases studied the second mechanism was the dominant one, although it should be true that there will be other combinations of shear and yaw angle at which the first mechanism is the most important.

Finally, there are several areas yet unresolved. The foremost is the quantification of the fluid-dynamical processes that set the circulation round the inlet and hence that determine the strength of the vortex generated by the second mechanism. If this can be done, one is then in a position to estimate which of the two mechanisms is important in a given situation, as well as how serious the vortex problem will be.

7. Summary and conclusions

Two basic mechanisms of inlet-vortex formation have been investigated experimentally and theoretically. The experimental study was conducted with a model inlet in a water tunnel using hydrogen-bubble flow visualization, while the theoretical investigation was based on a secondary-flow approach to calculating the three-dimensional vorticity field associated with this phenomenon.

The first of the two mechanisms is associated with the production of a vortex in a rotational flow that has a vertical component of ambient vorticity. It is the amplification of this vertical component (by stretching) as the vortex lines are drawn into the inlet that is responsible for the formation of an inlet vortex. The features of this amplification are shown by the calculations, which reveal that the three-dimensional motion (drift) of far-upstream vertical vortex filaments into the inlet results in a strong concentration of these filaments around the stagnation streamline

in front of the inlet. It is also found, however, that the presence of ambient vorticity is *not* essential for the generation of a vortex, and there is another, entirely different, mechanism for vortex formation. This second mechanism appears not to have been recognized previously. It can give rise to an inlet vortex in a flow that is (upstream) irrotational, for an inlet in cross wind. Associated with the inlet vortex in this situation is a variation in circulation along the length of the inlet and thus a trailing-vortex system.

An important parameter in determining the appearance of an inlet vortex is the ratio of inlet velocity to upstream velocity. In the first mechanism this ratio is important in the determination of the stretching incurred by a vertical vortex line and hence the vorticity amplification. In the second mechanism this ratio has a strong effect on the separation points on the inlet; consequently, it controls the inherent three-dimensionality of the flow directly, and, in particular, the circulation distribution along the inlet.

The experiments were carried out with an inlet and ground plane as well as with a twin-inlet configuration. The latter series of tests show that a ground boundary layer is not needed for the formation of an inlet vortex. Further, they present a situation in which an examination of the transient start-up process is extremely useful for understanding the fluid mechanics of the eventual steady state that is produced. Finally, they provide a clear illustration of the balance that can occur between vorticity production (by straining) within a fixed volume and the convection and diffusion of vorticity out of the volume.

The authors are grateful to Professors F. E. Marble of Caltech, Sir William Hawthorne of Cambridge University, H. W. Emmons of Harvard, and E. E. Covert of M.I.T., Drs N. A. Cumpsty and T. Hynes of Cambridge, Professor R. E. Mayle of RPI, and Mr J. P. Nikkanen of Pratt & Whitney Aircraft, for helpful discussions concerning different aspects of the fluid mechanics of inlet vortices. They also appreciate the suggestions of Professor A. H. Epstein with regard to various aspects of the experimental techniques used. In addition, they would like to thank Mr N. O. Stockman of NASA Lewis Research Center for making available the three-dimensional potential-flow code, and Dr J. Hess of McDonnell Douglas for his suggestions concerning its use. This work was supported by the Air Force Office of Scientific Research Contract no. F49620-78-C-0084, Program Manager Dr J. D. Wilson. One of the authors (H.C.V.) also acknowledges receipt of a Jean Gaillard Memorial Fellowship during 1979–1980.

Appendix. Changes of vorticity in a volume of fixed identity

In this appendix we derive an expression for the change of vorticity in a volume of fixed identity and apply this to a simple example, a vortex strained along its axis. We consider a constant-property fluid with no non-conservative body forces. For this situation, the curl of the momentum equation is

$$\frac{\partial \boldsymbol{\omega}}{\partial t} - \nabla \times (\mathbf{V} \times \boldsymbol{\omega}) = \nu \nabla \times (\nabla \times \boldsymbol{\omega}). \tag{A 1}$$

In (A 1) $\boldsymbol{\omega}$ is the vorticity, $\mathbf{V}$ is the velocity and ν is the kinematic viscosity. Integrating (A 1) over a *fixed* volume τ bounded by a fixed surface s gives

$$\int_\tau \frac{\partial \boldsymbol{\omega}}{\partial t} d\tau = \int_\tau \nabla \times (\mathbf{V} \times \boldsymbol{\omega})\, d\tau + \nu \int_\tau \nabla \times (\nabla \times \boldsymbol{\omega})\, d\tau. \tag{A 2}$$

This can be written as

$$\frac{\partial}{\partial t}\int_\tau \boldsymbol{\omega}\, d\tau = \underset{\text{(I)}}{\int_s (\hat{\mathbf{n}}\cdot\boldsymbol{\omega})\,\mathbf{V}\, ds} - \underset{\text{(II)}}{\int_s (\hat{\mathbf{n}}\cdot\mathbf{V})\,\boldsymbol{\omega}\, ds} - \underset{\text{(III)}}{\nu\int_s \hat{\mathbf{n}}\times(\nabla\times\boldsymbol{\omega})}. \tag{A 3}$$

Applying the divergence theorem to term (I), we obtain the desired expression for the *rate of change of vorticity in a fixed volume* τ:

$$\frac{\partial}{\partial t}\int_\tau \boldsymbol{\omega}\, d\tau = \underset{\text{(I)}}{\int_\tau (\boldsymbol{\omega}\cdot\nabla)\,\mathbf{V}\, d\tau} - \underset{\text{(II)}}{\int_s (\hat{\mathbf{n}}\cdot\mathbf{V})\,\boldsymbol{\omega}\, ds} - \underset{\text{(III)}}{\nu\int_s \hat{\mathbf{n}}\times(\nabla\times\boldsymbol{\omega})\, ds}. \tag{A 4}$$

The three terms show: (I) the production of vorticity inside the fixed volume by the stretching and 'tipping' of existing vortex lines; (II) the convection of vorticity out of the fixed volume through the fixed surface s; and (III) the diffusion of vorticity by viscous effects at the surface.

In the context of the present problem, it is of interest to apply (A 4) to the case of a vortex stretched along its axis at a constant strain rate β. As shown by Marble (1981 personal communications) (see also Batchelor 1967), this situation leads to an exact solution of the Navier–Stokes equations. With the geometry shown in the lower left on figure 23, the axial velocity V_z, the tangential velocity V_θ and the radial velocity V_r can be expressed as

$$V_z = \beta z, \quad V_\theta = \frac{\Gamma}{2\pi r}[1-\exp(-\beta r^2/4\nu)], \quad V_r = \tfrac{1}{2}\beta r, \quad \text{(A 5}a\text{), (A 5}b\text{), (A 5}c\text{)}$$

where β is a constant and Γ is the circulation. There is only an axial component of vorticity, whose magnitude is

$$\omega_z = \frac{\Gamma}{\pi}\exp(-\beta r^2/4\nu). \tag{A 6}$$

Substituting (A 5a–c) and (A 6) into (A 4) for a steady flow yields

$$0 = \underset{\text{(I)}}{2\pi\hat{k}\int_0^h\int_0^R \frac{\Gamma\beta}{\pi}\exp(-\beta r^2/4\nu)\, r\, dr\, dz} - \underset{\text{(II}a\text{)}}{2\pi h\hat{k}\int_0^R \frac{\Gamma\beta}{\pi}\exp(-\beta r^2/4\nu)\, r\, dr}$$
$$+ \underset{\text{(II}b\text{)}}{h\beta R^2\,\Gamma\exp(-\beta R^2/4\nu)\,\hat{k}} - \underset{\text{(III)}}{h\Gamma\beta R^2\exp(-\beta R^2/4\nu)\,\hat{k}}. \tag{A 7}$$

Equation (A 7) illustrates, for this particular situation, the balance between the production of vorticity and the convection of vorticity through the top A of the cylinder shown in figure 23, in terms (I) and (IIa), and the diffusion out and convection of vorticity in through the sides B of the cylinder, in terms (IIb) and (III). Note that, if the radius of the cylindrical control volume is taken to be large enough so that B is outside the region affected by viscosity, and hence terms (IIb) and (III) are negligible, the balance becomes one of production (inside) and convection through A, which is similar to the condition described in the body of the paper.

REFERENCES

BATCHELOR, G. K. 1967 *An Introduction to Fluid Mechanics*, chap. 5. Cambridge University Press.

BEARMAN, P. W. & ZDRAVKOVICH, M. M. 1978 Flow around a circular cylinder near a plane boundary. *J. Fluid Mech.* **89**, 33–47.

BISSINGER, N. C. & BRAUN, G. W. 1974 On the inlet vortex system. *NASA* CR-140182.

CLUTTER, D. W., SMITH, A. M. O. & BRAZIER, J. 1959 Techniques of flow visualization using water as the working medium. *Douglas Aircraft Co. Rep.* ES-29075.

COLEHOUR, J. L. & FARQUHAR, B. W. 1971 Inlet vortex. *J. Aircraft* **8**, 39–43.

DE SIERVI, F. 1981 A flow visualization study of the inlet vortex. *MIT Gas Turbine and Plasma Dynamics Lab. Rep.* no. 159.

GLENNY, D. E. 1970 Ingestion of debris into intakes by vortex action. *Min. of Tech., Aero. Res. Counc. CP* no. 1114.

GREITZER, E. M. 1980 Review – axial compressor stall phenomena. 1980 *Trans A.S.M.E.* I: *J. Fluids Engng* **102**, 134–151.

HAWTHORNE, W. R. 1965 Engineering aspects. In *Research Frontiers in Fluid Dynamics* (ed. R. J. Seeger & G. Temple), chap. 1. Wiley-Interscience.

HAWTHORNE, W. R. 1967 The applicability of secondary flow analysis to the solution of internal flow problems. In *Fluid Mechanics of Internal Flows* (ed. G. Sovran). Elsevier.

HESS, J. L. 1972 Calculation of potential flow about arbitrary three-dimensional lifting bodies. *McDonnell Douglas Rep.* MDC J5679-01.

HESS, J. L. 1974 The problem of three-dimensional lifting potential flow and its solution by means of surface singularity distribution. *Comp. Meth. in Appl. Mech. and Engng* **4**, 283–319.

HESS, J. L., MACK, D. & STOCKMAN, N. O. 1979 An efficient user-oriented method for calculating compressible flow in and about three-dimensional inlets. *McDonnell Douglas Rep.* no. MDC J7733; also *NASA* CR-15978.

HESS, J. L. & SMITH, A. M. O. 1966 Calculation of potential flow about arbitrary bodies. *Prog. Aero. Sci.* **8**, 1–138.

JOHNSON, F. T. 1980 A general panel method for the analysis and design of arbitrary configurations in incompressible flows. *NASA* CR-3079.

KERWIN, J. E. 1967 Variable pressure water tunnel. *MIT Dept of Naval Architecure Rep.*

KLEIN, H. 1957 An aerodynamic screen for jet engines. *Inst. of Aero Sci. Preprint* no. 676; presented at 25th Annual Meeting, 28–31 January 1957.

KOTANSKY, D. R. 1966 The use of honeycomb for shear flow generation. *A.I.A.A. J.* **4**, 1480–1491.

LIGHTHILL, M. J. 1956 Drift. *J. Fluid Mech.* **1**, 31–53.

LIGHTHILL, M. J. 1963 Boundary layer theory. In *Laminar Boundary Layers* (ed. L. Rosenhead), chap. II. Oxford University Press.

MATTINGLY, G. E. 1966 The hydrogen-bubble flow visualization technique. *David Taylor Model Basin Rep.* no. 2146.

MOTYCKA, D. L., WALTER, W. A. & MULLER, G. L. 1973 An analytical and experimental study of inlet ground vortices. *A.I.A.A. Paper* no. 73–1313.

MOTYCKA, D. L. & WALTER, W. A. 1975 An experimental investigation of ground vortex formation during reverse engine operation. *A.I.A.A. Paper* no. 75-1322.

MOTYCKA, D. L. 1976 Ground vortex-limit to engine/reverser operation. *Trans. A.S.M.E.* A: *J. Engng Power* **98**, 258–264.

NEWMAN, W. H. & ATASSI, H. 1980 A two-dimensional potential flow model for ground-induced effects on jet and fan inlets. *A.I.A.A. Paper* no. 80-0388.

RODERT, L. A. & GARRETT, F. B. 1953 Ingestion of foreign objects into turbine engines by vortices. *NACA* TN3330.

RUBBERT, P. E. 1977 Subsonic and supersonic panel methods. In *Applied Computational Aerodynamics*, A.I.A.A. Lecture Series.

SCHRAUB, F. A. *et al.* 1964 Use of hydrogen bubbles for quantitative determination of time dependent velocity fields in low speed water flows. *Rep.* MD-10, *Thermosci. Div., Dept Mech. Engng, Stanford Univ.*

VIGUIER, H. C. 1980 A secondary flow approach to the inlet vortex flow field. *MIT Gas Turbine Lab. Rep.* no. 155.